Title	Regnase-1 and Roquin Regulate a Common Element in Inflammatory mRNAs by Spatiotemporally Distinct Mechanisms.
Author(s)	Mino, Takashi; Murakawa, Yasuhiro; Fukao, Akira; Vandenbon, Alexis; Wessels, Hans-Hermann; Ori, Daisuke; Uehata, Takuya; Tartey, Sarang; Akira, Shizuo; Suzuki, Yutaka; Vinuesa, Carola G; Ohler, Uwe; Standley, Daron M; Landthaler, Markus; Fujiwara, Toshinobu; Takeuchi, Osamu
Citation	Cell (2015), 161(5): 1058-1073
Issue Date	2015-05-21
URL	http://hdl.handle.net/2433/197955
Right	© 2015 Elsevier Inc. Licensed under the Creative Commons Attribution-NonCommercial-NoDerivatives 4.0 International http://creativecommons.org/licenses/by-nc-nd/4.0/. NOTICE: this is the author's version of a work that was accepted for publication in Cell. Changes resulting from the publishing process, such as peer review, editing, corrections, structural formatting, and other quality control mechanisms may not be reflected in this document. Changes may have been made to this work since it was submitted for publication. A definitive version was subsequently published in Regnase-1 and Roquin Regulate a Common Element in Inflammatory mRNAs by Spatiotemporally Distinct Mechanisms. VOL.161, ISSUE.5, (2015) doi:10.1016/j.cell.2015.04.029.; 許諾条件により本文は2016-05-21に公開.
Type	Journal Article
Textversion	author

Regnase-1 and Roquin regulate a common element in inflammatory mRNAs by spatiotemporally distinct mechanisms

Takashi Mino[1,2], Yasuhiro Murakawa[3], Akira Fukao[4,12], Alexis Vandenbon[5,6], Hans-Hermann Wessels[3], Daisuke Ori[1,2], Takuya Uehata[1], Sarang Tartey[1,2], Shizuo Akira[7,8], Yutaka Suzuki[9], Carola G. Vinuesa[10], Uwe Ohler[3], Daron M. Standley[5,11], Markus Landthaler[3], Toshinobu Fujiwara[4,12], Osamu Takeuchi[1,2*]

[1]Laboratory of Infection and Prevention, [11]Laboratory of Integrated Biological Information, Institute for Virus Research, Kyoto University, [2]CREST, JST, Kyoto 606-8507, Japan

[3]Max Delbrück Center for Molecular Medicine, Berlin Institute for Medical Systems Biology, 13125 Berlin, Germany

[4]Laboratory of Hygienic Chemistry, Graduate School of Pharmaceutical Sciences, Nagoya City University, Nagoya 467-8603, Japan

[5]Laboratory of Systems Immunology, [6]Immuno-genomics Research Unit, [7]Laboratory of Host Defense, WPI Immunology Frontier Research Center, [8]Research Institute for Microbial Diseases, Osaka University, Suita, Osaka 565-0871, Japan

[9]Laboratory of Functional Genomics, Department of Medical Genome Sciences, Graduate School of Frontier Sciences, The University of Tokyo, Chiba 277-8562, Japan

[10]Department of Pathogens and Immunity, John Curtin School of Medical Research, Australian National University, Canberra, ACT 0200, Australia

[12]Present address; Department of Biochemistry, Faculty of Pharmacy, Kinki University, Higashiosaka, Osaka, 577-8502, Japan

*Correspondence: otake@virus.kyoto-u.ac.jp (O.T.)

Summary

Regnase-1 and Roquin are RNA binding proteins essential for degradation of inflammation-related mRNAs and maintenance of immune homeostasis. However, their mechanistic relationship has yet to be clarified. Here we show that although Regnase-1 and Roquin regulate an overlapping set of mRNAs via a common stem-loop structure, they function in distinct subcellular locations: ribosome/endoplasmic reticulum and processing-body/stress granules, respectively. Moreover, Regnase-1 specifically cleaves and degrades translationally active mRNAs and requires the helicase activity of UPF1, similar to the decay mechanisms of nonsense mRNAs. In contrast, Roquin controls translationally inactive mRNAs, independent of UPF1. Defects in both Regnase-1 and Roquin lead to large increases in their target mRNAs, although Regnase-1 tends to control the early phase of inflammation when mRNAs are more actively translated. Our findings reveal that differential regulation of mRNAs by Regnase-1 and Roquin depends on their translation status and enables elaborate control of inflammation.

Introduction

Inflammation is mediated by proinflammatory cytokines such as tumor necrosis factor (TNF) and Interleukin 6 (IL-6). Expression of cytokines is rapidly induced in response to infection by pathogens via Toll-like receptors (TLRs) in innate immune cells (Chovatiya and Medzhitov, 2014; Moresco et al., 2011; Takeuchi and Akira, 2010). Whereas cytokine mRNA levels are controlled at both transcriptional and post-transcriptional levels, post-transcriptional dampening of protein expression in particular can resolve inflammation and prevent unintended tissue damage (Anderson, 2010; Kafasla et al., 2014). Eukaryotic mRNAs are in dynamic equilibrium between different subcellular locations: actively translated mRNAs can be found in polysomes, mRNAs stalled in translation initiation can accumulate in stress granules (SGs), and mRNAs targeted for degradation or translation repression can accumulate in processing bodies (PBs). Further, mRNA-protein (mRNP) complexes dynamically move between polysomes, SGs and PBs (Anderson and Kedersha, 2009; Balagopal and Parker, 2009).

Many immune-related mRNAs have short half-lives because of conserved cis-elements including AU-rich elements (AREs) and stem-loop (SL) structures in their 3′ untranslated regions (UTRs) (Anderson, 2010; Kafasla et al., 2014). ARE binding proteins are involved in controlling the stability of such mRNAs. In addition, SLs present in mRNAs including ICOS, OX40 and TNF are destabilized by Roquin-1 and -2 (Leppek et al., 2013). These proteins harbor an RNA binding ROQ domain whose loss of function mutation (M199R) in mice (San) leads to the development of autoimmune disease characterized by an increase in follicular helper T cells (Linterman et al., 2009; Vinuesa et al., 2005; Yu et al., 2007). ARE- and Roquin-mediated mRNA decay takes place in PBs or SGs where a CCR4-CAF1-NOT deadenylase complex is recruited (Anderson, 2010; Athanasopoulos et al., 2010).

In contrast, another set of mRNA decay pathways target mRNAs undergoing translation. In the nonsense mediated decay (NMD), premature translation termination

at more than 20-25 bases 5′ of the exon junction complex (EJC) promotes the recruitment of an SMG1-UPF1-eRF1-eRF3 (SURF) complex (Kervestin and Jacobson, 2012; Popp and Maquat, 2013; Schweingruber et al., 2013). The SURF complex then interacts with the UPF2-UPF3-EJC complex, leading to recruitment of the endonucleases SMG6, SMG5 and SMG7, which mediate deadenylation for further degradation. In addition, active translation and UPF1 are required for some normal mRNA decay pathways, including staufen1-mediated mRNA decay (SMD) and replication-dependent histone mRNA decay (Kaygun and Marzluff, 2005; Kim et al., 2005).

We identified Regnase-1 (Reg1; also known as Zc3h12a and Mcpip1) as an RNase critical for preventing a severe autoimmune inflammatory disease in mice by destabilizing inflammation-related mRNAs (Iwasaki et al., 2011; Matsushita et al., 2009). Reg1 harbors a PIN-like RNase domain, and controls a set of genes including *Il6* and *Reg1* itself, but not *Nfkbia*, in macrophages following stimulation with TLR ligands such as lipopolysaccharide (LPS) and IL-1β, which activate shared signaling pathways. Reg1 is also essential for suppressing aberrant activation of T cells by targeting genes such as *Icos*, *c-Rel* and *Ox40* for degradation (Uehata et al., 2013).

In this study, we aim to uncover how Reg1 recognizes and degrades its target mRNAs, and show that Reg1 interacts with a set of SL-containing mRNAs that overlaps with those targeted by Roquin. In contrast to Roquin, Reg1 co-localizes with ribosomes, but not with PBs and SGs. Reg1 destabilizes translationally active mRNAs, and requires UPF1. The apparent cooperation between Reg1 and Roquin is confirmed by the upregulation of their mutual target mRNAs under mutation of both Reg1 and Roquin, although Reg1 and Roquin tend to control the early and late phases of inflammation, respectively. Thus, a common set of SL-containing mRNAs are recognized by distinct proteins in different stages of mRNA metabolism for fine tuning of immune responses.

Results

SL structure required for Reg1-RNA association.

We previously showed that a potential SL sequence in the *Il6* 3′UTR (84-102) is recognized by Reg1 for degradation (Matsushita et al., 2009). To determine the secondary structure of the *Il6* 3′UTR target sequence, we performed selective 2′-hydroxyl acylation analyzed by primer extension (SHAPE) analysis. The SHAPE results were consistent with the computational prediction of a simple SL structure with bulge (Figure 1A and 1B). We then examined if the SL is critical for the control of *Il6* expression by Reg1 by using an antisense morpholino that can interfere with SL formation in *Il6* 3′UTR (Il6-SL-MO) (Figure 1C). A luciferase assay expressing the reporter construct with the *Il6* 3′UTR, the morpholinos, and Reg1 revealed that the suppression of the luciferase activity observed in control (Ctrl) morpholino transfected cells was cancelled by the Il6-SL-MO (Figure 1D). Following introduction of the Il6-SL-MO to mouse bone marrow macrophages (BMMs), LPS-induced expression of mRNA and protein for IL-6, but not TNF, were significantly elevated compared with control cells (Figure 1E). We further supplemented *Il6*$^{-/-}$ mice with wild-type (WT) BMM treated with the Il6-SL-MO. LPS-induced production of IL-6, but not TNF, in the sera was elevated in mice supplemented with Il6-SL-MO-treated BMM, indicating that the SL in the *Il6* 3′ UTR is important for the regulation of IL-6 production *in vivo* (Figure 1F).

To investigate if the conserved SL is required for processing by Reg1, which harbors endonuclease activity as shown by the digestion of circular RNA *in vitro* (Figure S1A and S1B), we synthesized *Il6* 3′UTR RNAs with and without the SL (Figure S1C). Reg1 degraded RNAs harboring the SL, but not without the SL (Figure S1C), suggesting that the SL is required for RNase-mediated digestion or RNA binding. To distinguish between these two possibilities, we artificially tethered Reg1 to *Il6* coding and luciferase mRNAs using the λN-BoxB system (Figure 1G). Interestingly, a

λN-Reg1, but not WT Reg1, destabilized the *Il6* coding sequence in the presence of 5XBoxB in the Tet-off system (Figure 1H and 1I). This was further confirmed by a luciferase reporter assay expressing the luciferase construct with 5XBoxB in the 3′ UTR and λN-Reg1 (Figure S1D), indicating that the SL is required for the recruitment of target mRNAs by Reg1, but is dispensable for their degradation.

To check the possibility of Reg1-mediated control of miRNA generation (Suzuki et al., 2011), we prepared small RNAs from *Reg1*$^{-/-}$ mouse embryonic fibroblasts (MEFs). QPCR analysis revealed that the levels of miRNAs previously reported to be regulated by Reg1 as well as a set of LPS-inducible miRNAs including miR-155 and miR-146a did not increase in the absence of Reg1 (Figure S1E), indicating that Reg1 is dispensable for the control of these miRNAs.

Identification of mRNAs associating with Reg1.

To comprehensively identify mRNAs associated with Reg1, we performed RNA-immunoprecipitation (IP) sequencing (RIP-Seq) analysis. We expressed Flag-Reg1 lacking RNase activity (D141N), which was predicted to retain RNA binding activity (Figure S1F), in HeLa cells. We found that *IL6* and *Reg1* (*ZC3H12A*) were highly enriched by IP with Reg1 compared with control IP, both in unstimulated and IL-1β-stimulated cells (Figure 1J and Table S1), indicating that IP with Reg1 properly co-precipitated its target mRNAs. A total of 68 mRNAs were significantly enriched either in unstimulated or IL-1β-stimulated cells (p values < 10^{-3}) compared with control cells (Table S1). Gene ontology annotations enriched for the 68 Reg1-interacting mRNAs were often involved in inflammation (Table S2).

We then investigated if the Reg1-binding mRNAs were targeted by Reg1 for degradation. We constructed luciferase reporter genes with 3′UTRs from a set of enriched genes including *Nfkbiz*, *Nfkbid*, *Ptgs2*, *Mafk*, *Id1*, *Cxcl1*, *Cxcl2* and *Cxcl3*. Overexpression of Reg1 suppressed the luciferase activity in an RNase-activity

dependent manner (Figure 1K). Consistent with a previous report (Iwasaki et al., 2011), overexpression of Reg1 suppressed *Reg1* 3′ UTR containing nucleotides 1-210, but not in the case where nucleotides 1-200, which contains the SL, were absent. Collectively, Reg1-bound mRNAs obtained by RIP-Seq are indeed targeted by Reg1 for degradation.

The Reg1 target consensus motif overlaps with that of Roquin.

Roquin-1 was also reported to associate with SL containing mRNAs such as *Tnf*, *Icos*, *Nfkbid* and *Nfkbiz* in RAW264.7 cells (Leppek et al., 2013). Indeed, overexpression of Roquin suppressed the luciferase activity in the presence of the 3′UTR of *Nfkbiz*, *Nfkbid* and *Ptgs2* (Figure S1G), suggesting an overlap between Reg1 and Roquin target mRNAs.

We therefore next examined Roquin-interacting mRNAs globally in HeLa cells by RIP-Seq analysis. A total of 52 high-confidence mRNAs were enriched by IP with Flag-Roquin either in unstimulated or IL-1β-stimulated cells (p values < 0.01) (Table S3). Gene Set Enrichment Analysis (GSEA) showed that 68 Reg1 targets ($p \leq 1.0 \times 10^{-3}$) were significantly biased toward high enrichment scores (ES) in the Roquin RIP-seq data ($P < 1 \times 10^{-4}$; Figure 2A). We found a similar significant enrichment of Reg1 targets among mRNAs enriched in the Roquin RIP-seq sample when using the Kolmogorov-Smirnov test ($P < 2.2 \times 10^{-16}$). Reciprocally, the set of 52 high-confidence Roquin targets ($p \leq 0.01$) showed a significant overlap with mRNAs enriched in the Reg1 RIP-seq data ($P < 1 \times 10^{-4}$; Figure 2B). These 52 Roquin targets shared 10 mRNAs with the 68 Reg1 targets ($P = 2.69 \times 10^{-15}$). These results demonstrate that the Reg1 and Roquin target mRNAs overlap significantly.

Among newly identified Reg1-associated mRNAs, we focused on two mRNAs, *Nfkbiz* and *Ptgs2*. By testing luciferase constructs with truncated *Nfkbiz* 3′UTRs (Figure S2A), we found that *Nfkbiz* (100-150), which is evolutionally conserved and predicted to contain 2 SLs (Figure S2B and S2C), is required for Reg1-mediated suppression.

Addition of either one of these SL to the β-globin 3′UTR conferred responsiveness to Reg1 (Figure S2D). Similarly, we found that *Ptgs2* (1000-1300) was required for the regulation by Reg1 (Figure S2E). Mouse *Ptgs2* (1211-1228) was predicted and shown to form a conserved SL (Figure S2F-S2H), and this sequence alone was sufficient for Reg1 to suppress luciferase activity (Figure S2I). In addition, we found that a luciferase construct with the constitutive decay element (CDE) present in *Tnf* mRNA, which was identified as a Roquin target SL (Leppek et al., 2013), and SL alone (TNF-CDE37) was suppressed by Reg1 (Figure 2C and S2J).

Next, we investigated target structures present in Reg1 binding mRNAs globally by high-throughput sequencing of RNA isolated by crosslinking immunoprecipitation (HITS-CLIP) in HEK293 cells (chosen because of their wide usage in CLIP analysis) with stable, inducible expression of Flag-tagged WT Reg1 (Figure 2D). UV-crosslinked RNAs co-precipitated with Flag-Reg1 were recovered and sequenced. By analyzing sequence data of two biological replicate libraries, we identified 9107 and 10448 putative Reg1 binding groups in two biological duplicate libraries, respectively (Table S4). The two libraries intersected on a group level with at least one overlapping nucleotide; we thereby obtained 1143 Reg1 binding sites. As expected, many sites were located in 3′UTRs, although some fractions were mapped to coding regions and introns (Figure 2E). Although immune-related mRNAs were not frequently observed in HEK293 cells because of their poor expression, we identified Reg1 target sites in genes such as TM2D3, which was identified by RIP-seq analysis. The obtained sequences from them were predicted to form SLs (Figure 2F), and were suppressed by Reg1 (Figure 2G). When the Reg1 binding sequences were globally folded using RNAfold, SL structures with 3-7 nucleotide stems and 3 nucleotide loops were significantly enriched compared with 1000 individual permutations in both of the replicates and their intersection ($p < 0.001$) (Figure 2H). Next, we investigated the sequence motifs enriched in the Reg1 binding SLs harboring a hairpin of 3 nucleotides

with varying stem lengths (3, 5 or 7 nucleotides). Interestingly, the UAU sequence was significantly enriched in the hairpin sequences (Figure 2I).

Next, we examined the requirement of the SL structure and the specific hairpin loop sequence for Reg1-mediated target mRNA suppression. Using two validated SLs, TNF-CDE and another artificial SL with an UAU loop (Figure S3A-S3C), we first analyzed the importance of SL structures. Disruption of the SL structures abrogated Reg1-mediated suppression, and restoration of the SL structure by mutating both sides of the stem resulted in rescue of Reg1-mediated suppression (Figure S3D and S3E). We then generated a set of luciferase constructs harboring SLs with different loop sequences. In addition to SLs with UAU, UGU loop sequences were significantly inhibited by Reg1 overexpression (Figure 2J), indicating that SL sequences with either A or G at the second residue in the hairpin loop can be suppressed by Reg1. In contrast, ACA, AAA or UCU SLs were not suppressed by Reg1 expression, suggesting that a pyrimidine-purine-pyrimidine (Py-Pu-Py) sequence should be present in the loop.

Furthermore, IP with Reg1 co-precipitated reporter mRNA with a SL structure, while reporters whose SL was disrupted no longer co-precipitated with Reg1 (Figure S3F and S3G), indicating that the SL structure is required for Reg1 binding in cells. Additionally, alteration in the loop sequence abrogated its binding with Reg1 (Figure S3H).

Reciprocally, Roquin overexpression suppressed the luciferase activity and mRNA with β-globin 3′UTR followed by Reg1 target SL sequences (Figure 2K). Taken together, these results demonstrate that Reg1 and Roquin can recognize overlapping target mRNAs via the same SLs present in their 3′UTRs.

Reg1 localizes to the endoplasmic reticulum (ER), but not PBs or SGs.

The fact that Reg1 and Roquin recognize the same SL prompted us to investigate their relationship further. We first examined the involvement of deadenylation and decapping

in Reg1-mediated mRNA decay by overexpressing dominant negative mutants of Caf1 (Caf1-AA), and Dcp2 (Dcp2-AA). In contrast to Roquin-1 and -2, neither Caf1-AA nor Dcp2-AA affected Reg1-mediated degradation of *Il6* mRNA (Figure S4A).

We next investigated if Reg1 and Roquin function in the same subcellular location. Immunofluorescence staining revealed that Roquin-1 localizes in PBs in NIH3T3 and HeLa cells and in SGs upon arsenite treatment (Figure S4B and S4C). In contrast, NIH3T3 cells expressing Flag-Reg1 did not localize to PBs, or SGs upon arsenite treatment (Figure 3A and Figure S4D). In contrast, Reg1 co-localized with Calnexin, a type I membrane protein of the ER, but not with disulfide isomerase (PDI), a protein found within the ER (Figure 3B and S4E), indicating that Reg1 localizes on the surface of the ER. Because the surface of the rough ER (RER) is studded with ribosomes, we next demonstrated that Reg1 also co-localizes to the ribosome (Figure 3B and S4E). Moreover, immunoelectron microscopy analysis revealed that Reg1 localized to the cytoplasm and the surface of the ER (Figure 3C). Furthermore, subcellular fractionation of NIH3T3 cells revealed that endogenous Reg1 was present in the cytosol and RER, but not smooth ER, which does not contain ribosomes (Figure 3D).

To further investigate whether Reg1 localizes to translationally active polysomes, HeLa cell lysates were subjected to polysome fractionations (Figure 3E). Immunoblot analysis revealed that endogenous Reg1 localized in polysomal fractions in addition to non-polysome (non-ribosome and 40S-80S) fractions (Figure 3E), though Roquin-1 and -2 were localized in the non-polysome fractions.

Reg1, but not Roquin, regulates target mRNAs in the polysomal fraction.

Next we extracted RNAs from ribosomal fractions in HeLa cells following Reg1 and Roquin-1/-2 siRNA treatment with or without IL-1β stimulation, and examined the levels of mRNA expression in each fraction (Figure 3F and 3G). Reg1 and Roquin-1/-2

were efficiently suppressed at the mRNA and protein levels (Figure 3G and data not shown). Knockdown of Reg1 resulted in a large increase in *IL6* and *PTGS2* mRNA expression in the polysome fractions (fractions 7-12) compared with control cells, whereas the mRNA in non-polysome fractions (fractions 3-6) were comparable (Figure 3H). However, *TNF* and *NFKBIA* expression was unchanged in Reg1 knockdown. In contrast, *TNF* and *PTGS2* increased in Roquin-1/-2 knockdown cells. Interestingly, the increase was observed in non-polysome fractions, but not in polysome fractions (Figure 3H).

We further detected *PTGS2* in HeLa cells by using in situ hybridization following IL-1β stimulation (Figure S4F). Knockdown of Reg1 and Roquin-1/2 resulted in an increase in *PTGS2* expression (Figure S4F and S4G). Whereas Reg1 knockdown decreased *PTGS2* localized in the PB, Roquin-1/-2 knockdown increased *PTGS2* localized in PBs (Figure S4F and S4H). Taken together, these results demonstrate that Reg1 is critical for controlling the expression of translationally active mRNAs, whereas Roquin-1/2 regulate translationally inactive mRNAs in PBs/SGs.

Reg1 destabilizes translationally active mRNA via stop codons.

We next treated *Reg1*$^{-/-}$ macrophages with protein translation inhibitors, anisomycin and cycloheximide (CHX), and examined the kinetics of *Il6* and *Ptgs2* mRNA degradation after stimulation with LPS. Whereas *Il6* and *Ptgs2* mRNAs were stabilized in *Reg1*$^{-/-}$ macrophages compared with WT, the difference was lost following treatment with anisomycin or CHX (Figure 4A). Reciprocally, destabilization of *Il6* mRNA induced by Reg1 overexpression was no longer observed in response to treatment with these protein synthesis inhibitors (Figure 4B and 4C). The translation inhibitors did not alter Reg1 cellular localization or its protein expression levels (Figure S5A and S5B).

We next examined the effect of Reg1 on translationally inactive mRNA. We inserted a highly stable SL (SSL), which was shown to inhibit translation (Doma and

Parker, 2006), immediately upstream of the start codon of luciferase or *Il6* (Figure 4D). Insertion of the SSL to the luciferase reporter resulted in severe decrease in luciferase activity, but not in its mRNA, suggesting that the SSL suppressed protein synthesis (Figure 4E). Overexpression of Reg1 no longer destabilized *Il6* with the SSL in the 5′UTR (Figure 4F and 4G), further confirming that active translation is essential for Reg1-mediated mRNA decay.

However, Reg1-mediated mRNA destabilization was not affected by the presence of IRES at the 5′UTR (Figure S5C and S5D), suggesting that translation initiation is dispensable for the function of Reg1. In contrast, Reg1 failed to destabilize an *Il6* whose stop codons were mutated throughout the 3′UTR (*Il6* mRNA-ΔSTOP) and luciferase *Il6* 3′UTR without a stop codon (Figure 4F-4H). Requirement of stop codons in the Reg1-mediated mRNA decay prompted us to hypothesize that the distance between the stop codon and the *Il6* mRNA SL is important for Reg1–mediated destabilization. To examine this, we prepared *Il6* constructs harboring different distances between the stop codon and the SL (Figure 4I). Reg1 destabilized *Il6* mRNA with its original 3′UTR with (1-125), but not without (1-81), a SL (Figure 4J). Although the construct harboring the SL 23 bases downstream of the stop codon (64-125) was still suppressed by Reg1, those with the SL immediately downstream of the stop codon (82-125) were not (Figure 4J). These data suggest that the stop codon and SL structure require a minimal distance (about >20 nt) to be suppressed by Reg1.

Reg1 associates with ribosome proteins and UPF1.

Next we explored Reg1-associated proteins with a global proteomics approach using iTRAQ (Figure 5A). Levels of many ribosomal proteins in Reg1 immunoprecipitates from HeLa and RAW cells expressing Flag-Reg1 increased compared to control cells (Figure 5B and Table S5). Consistently, recombinant Reg1 precipitated by ultracentrifugation when incubated with highly-purified ribosome *in vitro* (Figure 5C),

suggesting that Reg1 is physically associated with the ribosome.

In addition to ribosomal proteins, we found that Flag-Reg1 co-precipitated UPF1 irrespective of Benzonase treatment (Figure 5B and 5D), suggesting that Reg1 and UPF1 exhibit direct protein-protein interaction. Whereas Reg1 lacking the N-terminal helical domain (90-596) (Figure 5E) was able to bind UPF1 (Figure 5F), Reg1 including the RNase domain to the C-terminal end (130-596) or only the C-terminal region (331-596) failed to co-precipitate UPF1 (Figure 5F). In contrast, Reg1 lacking the linker region between the N-terminal helical domain and the RNase domain (Δ90-130) showed severely impaired interaction with UPF1 (Figure 5F). Furthermore, overexpression of Reg1 (Δ90-130) lost the competency to suppress *Il6* and *Ptgs2* 3′UTR (Figure 5G), suggesting that the interaction between Reg1 and UPF1 is essential for Reg1 function.

UPF1 is critical for Reg1-mediated mRNA decay via its helicase activity.

Next we examined if UPF1 is required for Reg1-mediated decay. When we knocked down UPF1 in HEK293 cells, overexpressed Reg1 failed to degrade *Il6* (Figure 6A and 6B). Furthermore, Reg1 overexpression no longer suppressed the luciferase reporter constructs harboring 3′UTRs for *IL6*, *PTGS2*, *ICOS* and TNF-CDE37 in HeLa and RAW264.7 cells (Figure 6C and Figure S6A and S6B). In contrast, knockdown of UPF2 and UPF3x did not affect Reg1-mediated suppression (Figure 6C and Figure S6B). Further, the response to Roquin overexpression was not inhibited by the loss of UPF1 (Figure 6D and Figure S6C), indicating that Reg1 and Roquin degrade target mRNA in UPF1-dependent and –independent manners, respectively. Interestingly, knockdown of UPF1 or Reg1 in HeLa and RAW264.1 cells resulted in increased expression of *IL6* and *PTGS2*, but not *NFKBIA*, in response to IL-1β or LPS stimulation, respectively (Figure 6E and S6D). Knockdown of UPF1, but not Reg1, resulted in an increase in NMD-target genes such as *SMG5* and *GAS5* (Figure 6E and S6D).

Whereas overexpressed Reg1 co-precipitated *Il6*, UPF1 knockdown increased the amounts of *Il6* co-precipitated with Reg1 (Figure 6F). Knockdown of UPF1 abrogated Reg1-mediated inhibition, even when we tethered Reg1 to the target mRNA (Figure S6E and Figure 6G), indicating that UPF1 is required for Reg1 to cleave its target mRNAs after binding. Furthermore, anisomycin treatment abrogated the λN-Reg1-mediated suppression of *Il6*-5XBoxB expression (Figure 6H) without inhibiting the Reg1-*Il6* interaction (Figure S6F), indicating that translation is required for Reg1 to degrade associated mRNAs. The interaction between Reg1 and UPF1 was inhibited by the treatment with anisomycin (Figure 6I), suggesting that the association between Reg1 and UPF1 is mediated by translation.

We next examined the role of UPF1 helicase activity in controlling Reg1. We depleted endogenous UPF1 with siRNA and reconstituted it with exogenous siRNA-resistant WT and helicase inactive (D648A/E649A; DEAA) (Franks et al., 2010) mutant UPF1 in HeLa cells (Figure 6J). WT, but not the DEAA, rescued Reg1-mediated suppression of *Il6* 3′UTR (Figure 6K). Furthermore, IL-1β-mediated expression of *IL6* and *PTGS2* was suppressed by the UPF1 reconstitution in a manner dependent on the helicase activity (Figure 6L). Nevertheless, the UPF1 DEAA was capable of interacting with Reg1 (Figure S6G), indicating that the UPF1 helicase activity is required for Reg1 at the degradation step of its target mRNAs. Collectively, these results demonstrate that UPF1 interacts with Reg1 upon translation, and is essential for Reg1-mediated degradation of target mRNAs after recognition by acting as an RNA helicase.

Cooperative and distinct roles of Reg1 and Roquin in inflammatory gene expression.

Since Reg1 and Roquin suppress common target mRNAs via distinct molecular mechanisms, we investigated their relationship by expressing mutant Reg1 and Roquin in the same cells. First, we observed that the Reg1 D141N localized in SGs in addition

to ER following arsenite treatment (Figure S7A). Interestingly, the Reg1 D141N mutant cancelled suppression of luciferase reporter constructs harboring 3′UTRs for *Il6* (86-102) and *Ptgs2* 3′UTR by Roquin overexpression (Figure S7B). In contrast, Roquin-NT, whose localization is consistent with WT Roquin (data not shown), failed to alter Reg1-mediated suppression (Figure S7B). These results suggest that Reg1 and Roquin affect the same SL, and that the Reg1 D141N mutant stays on the 3′UTR and thereby inhibits the action of Roquin.

We further examined the roles of Reg1 and Roquin by generating BMMs harboring *Reg1*$^{-/-}$ and *Roquin-1*$^{San/San}$ alleles. We found that the expression of *Il6* and *Tnf* upon LPS stimulation was augmented in *Reg1*$^{-/-}$ and *Roquin-1*$^{San/San}$ BMM, respectively (Figure 7A). Further, *Ptgs2* mRNA increased in *Reg1*$^{-/-}$ and *Roquin-1*$^{San/San}$ BMM. Since *Il6*, *Tnf* and *Ptgs2* mRNAs present in polysomal fractions rapidly increased in response to IL-1β stimulation in HeLa cells and then decreased at later time points (Figure 3H and S7C), we hypothesized that the contribution of translation-dependent decay by Reg1 changes in the time-course of BMM activation. Indeed, the difference in *Il6* and *Ptgs2* expression between WT and *Reg1*$^{-/-}$ BMM was more obvious 1 or 2 h after LPS stimulation than 8 h post stimulation (Figure 7A). In contrast, the difference in *Tnf* and *Ptgs2* expression in WT and *Roquin-1*$^{San/San}$ BMM was greater 4 and 8 h after LPS than at earlier time points. These data demonstrate that Reg1 and Roquin play more important roles earlier and later, respectively, in response to TLR stimulation. Consistent with the *Ptgs2* mRNA expression results, Ptgs2 protein was expressed more abundantly in *Reg1*$^{-/-}$ BMM 2 h after LPS stimulation compared with WT (Figure 7B). In contrast, the expression of Ptgs2 protein in *Roquin-1*$^{San/San}$ BMM increased greatly 8 h after stimulation. Furthermore, the Ptgs2 protein/mRNA ratio was higher in *Reg1*$^{-/-}$ BMM compared with WT and *Roquin-1*$^{San/San}$ cells (Figure 7C). These results are consistent with the increased expression of *Ptgs2* mRNAs in polysomal fractions in HeLa cells with defective expression of Reg1 (Figure 3H).

Although *Reg1*$^{-/-}$; *Roquin-1*$^{San/San}$ double mutant mice were mostly embryonic lethal (data not shown), we successfully established MEFs with the *Reg1*$^{-/-}$; *Roquin*$^{San/San}$ genotype. In response to LPS and TNF stimulation in WT MEFs, the expression of genes including *Il6*, *Tnf* and *Ptgs2* was upregulated (Figure 7D and S7D). MEFs lacking Reg1 showed increased expression of *Il6* and *Ptgs2* compared with WT, particularly in the early phase of the responses (Figure 7D). Similarly, the Roquin San mutation resulted in an increase in the expression of *Tnf*, *Il6* and *Ptgs2* at later time points after LPS stimulation (Figure 7D). Interestingly, *Reg1*$^{-/-}$; *Roquin*$^{San/San}$ MEFs showed high increases in the expression of *Il6*, *Tnf* and *Ptgs2* mRNAs both in early and late phases, suggesting that Reg1 and Roquin in part redundantly regulate their target mRNAs, although *Nfkbia* expression was not altered (Figure 7D and S7D).

Finally, we examined the genome-wide changes in gene expression in WT, *Reg1*$^{-/-}$, *Roquin-1*$^{San/San}$ and *Reg1*$^{-/-}$; *Roquin-1*$^{San/San}$ MEFs with or without LPS stimulation by transcriptome analysis (Table S6). A set of genes was greatly increased in *Reg1*$^{-/-}$; *Roquin-1*$^{San/San}$ double mutant MEFs compared with WT (Figure S7E). GSEA revealed that the mouse counterparts of Reg1- and Roquin-binding mRNAs identified by RIP-sequencing analysis were significantly enriched in genes more abundantly expressed in *Reg1*$^{-/-}$; *Roquin-1*$^{San/San}$, *Reg1*$^{-/-}$ and *Roquin-1*$^{San/San}$ MEFs (Figure 7E, 7F and Figure S7F). These results indicate that the Reg1- and Roquin-binding mRNAs are commonly regulated by these RNA binding proteins.

Discussion

In this study, we found that Reg1 and Roquin target overlapping mRNAs and SLs for degradation. Nevertheless, they degrade the target mRNAs using different molecular mechanisms and in different cellular locations. Whereas Roquin localizes in PBs/SGs and degrades mRNAs via deadenylation like other mRNA decay pathways, Reg1 associates with ribosomes, and degrades mRNAs in a translation-dependent manner (Figure 7G).

The UAU loop sequence was enriched in Reg1-binding sites, and the loop sequence was important for Reg1-mediated mRNA decay. So far, all validated Reg1 target SLs contain a Py-Pu-Py loop sequence, and mutation of this loop sequence results in Reg1 unresponsiveness, a rule shared by Roquin target mRNAs. We did not find a specific rule in the stem-sequence of Reg1-target mRNAs, although Roquin target stem sequences were reported to harbor the UUG sequence in their upper stem. One possibility is that Reg1 can recognize a broader range of SL structures than Roquin. However, crystal structures studies revealed that Roquin ROQ domain interacts with the TNF-CDE stem and a triloop with Py-Pu-Py sequences, and that Roquin uses mainly non-sequence-specific contacts with the RNA (Schlundt et al., 2014; Schuetz et al., 2014; Tan et al., 2014). Indeed, we found that overexpression of Roquin could affect 3′ UTRs harboring a stem without the UUC sequence. Therefore, the requirement for particular stem sequences may not be so strict, and SL structures harboring a Py-Pu-Py loop sequence might be more broadly recognized by both Reg1 and Roquin.

Reg1 and Roquin negatively regulate activation of T cells in addition to the control of inflammatory gene expression in innate immune cells (Pratama et al., 2013; Uehata et al., 2013; Vogel et al., 2013). *Icos* is a common target of Reg1 and Roquin proteins, and we found that a SL structure present in its 3′UTR is recognized by both Reg1 and Roquin. A recent report showed that *Nfkbiz* and *Nfkbid* are suppressed by Reg1 and Roquin in T cells, controlling Th17 differentiation, although their relationship

was not studied (Jeltsch et al., 2014). We focused on the mechanisms in innate immune and non-immune cells in this study; however, it is likely that Reg1 and Roquin similarly regulate mRNAs related to T cell activation in a manner dependent on the state of translation. Since lethality upon mutation of both Reg1 and Roquin prohibited analyzing their roles in adult T cells, it would be interesting to analyze their functional roles in T cells by using conditional alleles in the future.

We found that Reg1-mediated mRNA decay requires translation and translation termination approximately 20 bases or more upstream of the SL. Similar to NMD, the stop codon might be required for preventing the disruption of the SL by the ribosome. In addition, the requirement of UPF1 demonstrates that the Reg1-mediated decay mechanism is highly similar to that of the quality control pathway, NMD. In the execution of NMD, endonucleolytic cleavage by SMG6 as well as exonucleolytic cleavage induced by the complex of SMG5-SMG7 contributes to the degradation of aberrant mRNAs (Eberle et al., 2009; Loh et al., 2013). SMG6-cleaved mRNA product can be further degraded in a manner dependent on the exosome and XRN1 exonucleases. Since Reg1 serves as an endonuclease like SMG6, a similar complete mRNA degradation system might operate upon cleavage by Reg1.

An open question is why Reg1-mediated mRNA decay requires active translation. Given that translation-inactive mRNAs are not affected by the absence of Reg1, this mechanism may be beneficial for maintaining a certain reserve of inflammation-related mRNAs. If Reg1 were to arbitrarily degrade its target mRNAs irrespective of their translation status, immune-related mRNA levels might become very low and additional energy would be required for de novo transcription. Alternatively, this mechanism may lead to the production of one protein per mRNA to keep control of short half-lives of Reg1-target mRNAs. In contrast, Roquin-mediated decay is involved in the constitutive decay of mRNAs and can be important for the regulation of the amounts of stored immune-related mRNAs. The presence of different regulatory

proteins makes posttranslational control of inflammation more elaborate than previously realized.

Although UPF1 is essential for NMD, the molecular mechanisms how UPF1 is involved in NMD are still under debate. In one model, UPF1 is recruited to the mRNP complex upon translation termination forming a SURF complex (Kurosaki and Maquat, 2013), and the helicase activity of UPF1 is proposed to be required for the disassembly of the mRNP complex (Franks et al., 2010). However, this model was challenged in reports demonstrating that UPF1 is associated with mRNAs even before translation (Hogg and Goff, 2010; Hurt et al., 2013; Zund et al., 2013). The helicase activity of UPF1 is essential for Reg1-mediated cleavage of target mRNAs, although this activity is dispensable for Reg1 to interact with its target mRNAs. Therefore, the Reg1-UPF1 interaction is possibly induced in the course of translation irrespective of UPF1 helicase activity, which may potentiate the RNase activity of Reg1 by remodeling an mRNP complex (Figure 7G).

Reg1-mediated decay is dependent on UPF1, but not on UPF2 and UPF3x. Whereas all three UPF members are required for NMD, UPF2 and UPF3x are also dispensable for SMD and replication-dependent histone mRNA decay (Kaygun and Marzluff, 2005; Kim et al., 2005). Nevertheless, Staufen 1 and 2 are sensors for recognizing dsRNA sequences (Park et al., 2013), but do not have RNase activity. Staufen1 was dispensable for the Reg1-mediated decay (data not shown), and Reg1-mediated mRNA decay is highly unique in that Reg1 serves as both a sensor for the SL and a degradation enzyme simultaneously.

Although loss of function of both Reg1 and Roquin-1/-2 resulted in a large increase in the expression of *Tnf*, *Il6* and *Ptgs2*, dysfunction of Reg1 or Roquin alone seems to differentially regulate *Il6* and *Tnf*, respectively. Further, both Reg1 and Roquin-1 suppressed *Tnf* and *Il6* mRNA 3′ UTRs upon overexpression; thus, it is currently difficult to explain why *Tnf* expression did not increase under Reg1 deficiency.

Since Reg1 is critical for the regulation of *Tnf* in the absence of Roquin, Roquin may bind with the *Tnf* SL more strongly than Reg1 and thus reduce the accessibility of Reg1 to *Tnf* mRNA. Furthermore, it would not be surprising if the translation status dynamically changes in the course of the life of an mRNA. Further studies will uncover the mechanisms of dynamic cellular regulation of mRNA translation status in relation to mRNA decay.

Collectively, this study clearly demonstrates that the posttranscriptional regulation of inflammation is controlled by Reg1 and Roquin in spatiotemporally distinct manners. Given that excess and prolonged production of cytokines leads to the onset of inflammatory diseases, prolonged stability of inflammatory cytokine mRNAs can be considered aberrant, and thus targeted by the quality control system. Differential regulation of Reg1- and Roquin-mediated mRNA degradation are thus necessary for the elaborate control of inflammation.

Experimental Procedures

RIP-sequencing

HeLa expressing Flag-Reg1-D141N, Roquin-1 or an empty vector were stimulated with human IL-1β (10 ng/mL) for 2 h. RNA-protein complexes were immunoprecipitated with anti-Flag antibody (F3165; Sigma) bound to protein G magnetic beads and RNAs were extracted from the beads. RNA library was prepared using Small RNA Sample Prep kit v1.0 (Illumina Inc.) and sequenced on a HiSeq 2000 system (Illumina) also according to the manufacturer's instructions. The resulting set of trimmed reads were then mapped against the human genome (hg19; NCBI).

mRNA decay assay

For mRNA decay experiments with Tet-off system, doxycycline (1 μg/ml) (Sigma) was added to the medium for the indicated time intervals before harvesting Tet-off 293 cells. Total RNA was isolated using Trizol (Invitrogen). mRNA levels were determined either by northern blot or by RT-qPCR analysis. For determining RNA decay using the Click-iT® Nascent RNA Capture Kit (Invitrogen), peritoneal macrophages were labelled with EU (0.5 mM) and stimulated with LPS (100 ng/mL) for 2 hr and the medium was replaced with growth medium without EU for the indicated time intervals before harvesting EU-labeled peritoneal macrophages. EU-labeled RNAs (EU-RNAs) were biotinylated and the biotinylated RNAs were purified with streptavidin magnetic beads and analyzed with RT-qPCR.

Luciferase assay

HeLa cells were transfected with luciferase reporter plasmid pGL3 containing the 3′ UTR of indicated genes, together with expression plasmid for Regnase-1 or empty (control) plasmid. After 24 h of cultivation, cells were lysed and luciferase activity in lysates was determined with the Dual-Luciferase Reporter Assay system (Promega).

The gene encoding Renilla luciferase was transfected simultaneously as an internal control.

Statistical analysis

Data are presented as means ± standard deviation. Statistical significance was calculated with a Student's t-test. Significance was accepted at the level of $P < 0.05$ (*), $P < 0.01$ (**) or $P < 0.001$ (***).

Materials and experimental procedures are detailed in the Extended Experimental Procedures.

Author Contributions

T.M. and O.T. designed the research, performed experiments and wrote the paper.

Y.M., H.H.W., U.O. and M.L. performed CLIP analysis.

A.F. and T.F. performed polysome fractionation and ribosome-binding assay.

A.V. and D.M.S. carried out bioinformatics analysis.

D.O., T.U., S.T. S.A., Y.S. and C.G.V. helped with experiments.

Acknowledgments

We thank G Stoecklin, A Yamashita and Y Mishima for plasmids; K Saito, H Omori, M Kitabatake and M Ohno for experiments. We thank all members of our laboratory for discussions.

This work was supported by the JSPS through Core-to-Core Program, Grant-in-Aid for Young Scientists (B) (to T.M.), for Scientific Research on Innovative Areas ‘‘Genome Science’’ (221S0002), and grants from Takeda Science Foundation, Daiichi Sankyo Foundation of Life Science (to O.T.), and the Shimizu Foundation for Immunology and Neuroscience (to T.M.).

Accession Numbers

All data have been deposited at DDBJ: DRA003232 for Table S1, DRA003233 for Table S3, DRA003463 for Table S4 and DRA003234 for Table S6.

References

Anderson, P. (2010). Post-transcriptional regulons coordinate the initiation and resolution of inflammation. Nat Rev Immunol *10*, 24-35.

Anderson, P., and Kedersha, N. (2009). RNA granules: post-transcriptional and epigenetic modulators of gene expression. Nat Rev Mol Cell Biol *10*, 430-436.

Athanasopoulos, V., Barker, A., Yu, D., Tan, A.H., Srivastava, M., Contreras, N., Wang, J., Lam, K.P., Brown, S.H., Goodnow, C.C., *et al.* (2010). The ROQUIN family of proteins localizes to stress granules via the ROQ domain and binds target mRNAs. FEBS J *277*, 2109-2127.

Balagopal, V., and Parker, R. (2009). Polysomes, P bodies and stress granules: states and fates of eukaryotic mRNAs. Curr Opin Cell Biol *21*, 403-408.

Chovatiya, R., and Medzhitov, R. (2014). Stress, Inflammation, and Defense of Homeostasis. Mol Cell *54*, 281-288.

Doma, M.K., and Parker, R. (2006). Endonucleolytic cleavage of eukaryotic mRNAs with stalls in translation elongation. Nature *440*, 561-564.

Eberle, A.B., Lykke-Andersen, S., Muhlemann, O., and Jensen, T.H. (2009). SMG6 promotes endonucleolytic cleavage of nonsense mRNA in human cells. Nat Struct Mol Biol *16*, 49-55.

Franks, T.M., Singh, G., and Lykke-Andersen, J. (2010). Upf1 ATPase-dependent mRNP disassembly is required for completion of nonsense- mediated mRNA decay. Cell *143*, 938-950.

Hogg, J.R., and Goff, S.P. (2010). Upf1 senses 3'UTR length to potentiate mRNA decay. Cell *143*, 379-389.

Hurt, J.A., Robertson, A.D., and Burge, C.B. (2013). Global analyses of UPF1 binding and function reveal expanded scope of nonsense-mediated mRNA decay. Genome Res *23*, 1636-1650.

Iwasaki, H., Takeuchi, O., Teraguchi, S., Matsushita, K., Uehata, T., Kuniyoshi, K., Satoh, T., Saitoh, T., Matsushita, M., Standley, D.M., *et al.* (2011). The IkappaB kinase complex regulates the stability of cytokine-encoding mRNA induced by TLR-IL-1R by controlling degradation of regnase-1. Nat Immunol *12*, 1167-1175.

Jeltsch, K.M., Hu, D.S., Brenner, S., Zoller, J., Heinz, G.A., Nagel, D., Vogel, K.U., Rehage, N., Warth, S.C., Edelmann, S.L., *et al.* (2014). Cleavage of roquin and regnase-1 by the paracaspase MALT1 releases their cooperatively repressed targets to promote T(H)17 differentiation. Nature Immunology *15*, 1079-1089.

Kafasla, P., Skliris, A., and Kontoyiannis, D. (2014). Post-trascriptional coordination of immunological responses by RNA-binding proteins. Nat Immunol *15*, 492-502.

Kaygun, H., and Marzluff, W.F. (2005). Regulated degradation of replication-dependent histone mRNAs requires both ATR and Upf1. Nat Struct Mol Biol *12*, 794-800.

Kervestin, S., and Jacobson, A. (2012). NMD: a multifaceted response to premature translational termination. Nat Rev Mol Cell Biol *13*, 700-712.

Kim, Y.K., Furic, L., Desgroseillers, L., and Maquat, L.E. (2005). Mammalian Staufen1 recruits Upf1 to specific mRNA 3'UTRs so as to elicit mRNA decay. Cell *120*, 195-208.

Kurosaki, T., and Maquat, L.E. (2013). Rules that govern UPF1 binding to mRNA 3' UTRs. Proc Natl Acad Sci U S A *110*, 3357-3362.

Leppek, K., Schott, J., Reitter, S., Poetz, F., Hammond, M.C., and Stoecklin, G. (2013). Roquin promotes constitutive mRNA decay via a conserved class of stem-loop recognition motifs. Cell *153*, 869-881.

Linterman, M.A., Rigby, R.J., Wong, R.K., Yu, D., Brink, R., Cannons, J.L., Schwartzberg, P.L., Cook, M.C., Walters, G.D., and Vinuesa, C.G. (2009). Follicular helper T cells are required for systemic autoimmunity. J Exp Med *206*, 561-576.
Loh, B., Jonas, S., and Izaurralde, E. (2013). The SMG5-SMG7 heterodimer directly recruits the CCR4-NOT deadenylase complex to mRNAs containing nonsense codons via interaction with POP2. Genes Dev *27*, 2125-2138.
Matsushita, K., Takeuchi, O., Standley, D.M., Kumagai, Y., Kawagoe, T., Miyake, T., Satoh, T., Kato, H., Tsujimura, T., Nakamura, H., *et al.* (2009). Zc3h12a is an RNase essential for controlling immune responses by regulating mRNA decay. Nature *458*, 1185-1190.
Moresco, E.M., LaVine, D., and Beutler, B. (2011). Toll-like receptors. Curr Biol *21*, R488-493.
Park, E., Gleghorn, M.L., and Maquat, L.E. (2013). Staufen2 functions in Staufen1-mediated mRNA decay by binding to itself and its paralog and promoting UPF1 helicase but not ATPase activity. Proc Natl Acad Sci U S A *110*, 405-412.
Popp, M.W., and Maquat, L.E. (2013). Organizing principles of mammalian nonsense-mediated mRNA decay. Annu Rev Genet *47*, 139-165.
Pratama, A., Ramiscal, R.R., Silva, D.G., Das, S.K., Athanasopoulos, V., Fitch, J., Botelho, N.K., Chang, P.P., Hu, X., Hogan, J.J., *et al.* (2013). Roquin-2 shares functions with its paralog Roquin-1 in the repression of mRNAs controlling T follicular helper cells and systemic inflammation. Immunity *38*, 669-680.
Schlundt, A., Heinz, G.A., Janowski, R., Geerlof, A., Stehle, R., Heissmeyer, V., Niessing, D., and Sattler, M. (2014). Structural basis for RNA recognition in roquin-mediated post-transcriptional gene regulation. Nat Struct Mol Biol *21*, 671-678.
Schuetz, A., Murakawa, Y., Rosenbaum, E., Landthaler, M., and Heinemann, U. (2014). Roquin binding to target mRNAs involves a winged helix-turn-helix motif. Nat Commun *5*, 5701.
Schweingruber, C., Rufener, S.C., Zund, D., Yamashita, A., and Muhlemann, O. (2013). Nonsense-mediated mRNA decay - mechanisms of substrate mRNA recognition and degradation in mammalian cells. Biochim Biophys Acta *1829*, 612-623.
Suzuki, H.I., Arase, M., Matsuyama, H., Choi, Y.L., Ueno, T., Mano, H., Sugimoto, K., and Miyazono, K. (2011). MCPIP1 ribonuclease antagonizes dicer and terminates microRNA biogenesis through precursor microRNA degradation. Mol Cell *44*, 424-436.
Takeuchi, O., and Akira, S. (2010). Pattern recognition receptors and inflammation. Cell *140*, 805-820.
Tan, D., Zhou, M., Kiledjian, M., and Tong, L. (2014). The ROQ domain of Roquin recognizes mRNA constitutive-decay element and double-stranded RNA. Nat Struct Mol Biol *21*, 679-685.
Uehata, T., Iwasaki, H., Vandenbon, A., Matsushita, K., Hernandez-Cuellar, E., Kuniyoshi, K., Satoh, T., Mino, T., Suzuki, Y., Standley, D.M., *et al.* (2013). Malt1-induced cleavage of regnase-1 in CD4(+) helper T cells regulates immune activation. Cell *153*, 1036-1049.
Vinuesa, C.G., Cook, M.C., Angelucci, C., Athanasopoulos, V., Rui, L., Hill, K.M., Yu, D., Domaschenz, H., Whittle, B., Lambe, T., *et al.* (2005). A RING-type ubiquitin ligase family member required to repress follicular helper T cells and autoimmunity. Nature *435*, 452-458.
Vogel, K.U., Edelmann, S.L., Jeltsch, K.M., Bertossi, A., Heger, K., Heinz, G.A., Zoller, J., Warth, S.C., Hoefig, K.P., Lohs, C., *et al.* (2013). Roquin paralogs 1 and 2

redundantly repress the Icos and Ox40 costimulator mRNAs and control follicular helper T cell differentiation. Immunity *38*, 655-668.
Yu, D., Tan, A.H., Hu, X., Athanasopoulos, V., Simpson, N., Silva, D.G., Hutloff, A., Giles, K.M., Leedman, P.J., Lam, K.P*., et al.* (2007). Roquin represses autoimmunity by limiting inducible T-cell co-stimulator messenger RNA. Nature *450*, 299-303.
Zund, D., Gruber, A.R., Zavolan, M., and Muhlemann, O. (2013). Translation-dependent displacement of UPF1 from coding sequences causes its enrichment in 3' UTRs. Nat Struct Mol Biol *20*, 936-943.

Figure Legends

Figure 1. Identification of Reg1 target mRNAs

(A) SHAPE analysis of *in vitro* synthesized Il6 3′UTR (84-103) RNA.

(B and C) Schematic representation of Il6 3′UTR-(84-103) (B), and *Il6* 3′UTR and antisense morpholinos (C).

(D) HeLa cells were transfected with the *Il6* 3′UTR reporter, antisense morpholinos, and Reg1 expression plasmids. The luciferase activities are shown as relative values.

(E) Ctrl- and Il6-SL-MO were delivered into WT BMMs followed by stimulation with LPS. Cytokine mRNA (top) and protein (bottom) levels were analyzed by RT-qPCR and ELISA, respectively.

(F) WT BMMs delivered with antisense morpholinos were i.p. transfused into *Il6*$^{-/-}$ mice (6-week-old, n = 4). The mice were i.p. injected with LPS (0.5 mg/kg of BW). Cytokine levels in sera were measured by ELISA 24 h after transfusion.

(G) Schematic representation of λN-BoxB tethering system.

(H) Tef-off 293 cells were transfected with pTRE-Il6CDS-5XBoxB and indicated expression plasmids. Total RNAs were prepared after Dox treatment, and *Il6* levels were determined by Northern blot analysis.

(I) Immunoblot analysis of Reg1 in HeLa cells transfected with indicated expression plasmids.

(J) Correlation of ppm between control IP samples (x axis) and Reg1 IP samples (y axis). mRNAs associated with Reg1 in IL-1β-stimulated HeLa cells were determined by RIP-seq.

(K) Luciferase activity of HeLa cells transfected with reporter plasmids expressing 3′UTR of indicated genes and Reg1 expression plasmids.

Unless otherwise indicated, Data are mean ± SD (n = 3). See also Figures S1 and Table S1 and S2.

Figure 2. Identification of the consensus sequences of the Reg1 target mRNAs and their overlap with Roquin

(A and B) GSEA of overlap between Reg1 and Roquin target genes (RIP-seq based). ES plots are shown with genes ranked according to their Roquin (A) and Reg1 (B) RIP-seq p values. The right part shows the histogram for the max ES scores.

(C, G, J, K) Luciferase activity of HeLa cells transfected with indicated reporter, Reg1 and Roquin expression plasmids. Data are mean ± SD (n = 3).

(D) Phosphorimages of NuPAGE gels that resolved 5′-[^{32}P]-labelled RNA–Flag-Reg1 IP. Lower panels show immunoblots for Reg1.

(E) Proportion of Reg1 binding sites obtained by the intersection of two biological HITS-CLIP replicates.

(F) Schematic representation of TM2D3 (95-120).

(H) SL enrichment in Reg1 bound CLIP tags in 3′UTRs compared to 1000 individual sequence permutations. The bar color represents the p value corresponding to the enrichment.

(I) Description of significantly enriched Reg1 bound SLs harboring a hairpin of 3 nucleotides with varying stem length (3, 5 or 7 nucleotides). Representation of SL sequence as Position Weight Matrix (PWM) logos. Logos are centered on the hairpin midpoint. Letter scale corresponds to relative nucleotide entropy.

See also Figure S2 and S3, and Table S3 and S4.

Figure 3. Reg1 localizes to ER and polysome fraction

(A, B) NIH3T3 cells expressing Flag-Reg1 were treated with arsenite and analyzed by confocal fluorescence microscopy.

(C) Immunoelectron microscopy showing the localization of Reg1 in NIH3T3 cells. The black arrows indicate Reg1 localized at surface of ER. Scale bar, 1 μm. mt, mitochondria.

(D) Subcellular fractions of Reg1 prepared from NIH3T3 cells were analyzed by Immunoblotting.

(E) The lysates from HeLa cells were fractionated by sucrose gradient. The expression of Reg1 and Roquin in the fractions was analyzed by Immunoblotting.

(F–H) Quantification of RNAs of non-polysome and polysome fractions. The lysates from HeLa cells transfected with indicated siRNA and stimulated with IL-1β were fractionated by sucrose gradient (F) and RNAs from the fractions were analyzed by RT-qPCR for the expression of indicated mRNAs (G, H). Data are mean ± SD (n = 3).

See also Figure S4.

Figure 4. Translationally active mRNAs are targeted by Reg1 via the stop codon

(A) WT and *Reg1*$^{-/-}$ macrophages were labelled with EU, stimulated with LPS and treated with anisomycin or CHX for 2 hr. EU-labeled *Il6* and *Ptgs2* mRNAs were captured by the Click-iT Nascent RNA Capture Kit and measured by RT-qPCR.

(B and C) Tef-off 293 cells were co-transfected with pTRE-Il6 CDS-3′UTR and indicated expression plasmids. Cells were then treated with anisomycin or CHX, and RNAs were prepared after Dox treatment, and *Il6* mRNA levels were determined by Northern blot analysis (B) and the autoradiographs were quantified (C).

(D) Schematic representation of SSL-inserted mRNAs.

(E) The SSL inhibited luciferase activity, but not its mRNA expression.

(F and G) Degradation of *Il6*, SSL-inserted *Il6* and stop codon-deleted (ΔSTOP) *Il6* by Reg1 was measured as in (B) (F), and the autoradiographs were quantified (G).

(H) Luciferase activity of HeLa cells transfected with the *Il6* reporter lacking a stop codon and Reg1 expression plasmids.

(I and J) Schematic representation of deletion mutants of *Il6* 3'UTR (I). Degradation of *Il6* mutant mRNAs was measured and quantified (J).

Unless otherwise indicated, Data are mean ± SD (n = 3).

See also Figure S5.

Figure 5. Reg1 interacts with Ribosome proteins and UPF1

(A) Schematic representation of the iTRAQ workflow.

(B) Proteins enriched by iTRAQ-based proteomics identifying Reg1-associated proteins.

(C) Recombinant Reg1 co-precipitated with ribosome purified from HeLa cells was analyzed by SDS-PAGE.

(D and F) Immunoblot analysis of UPF1 co-precipitated with Flag-Reg1-WT and D141N (D) or its deletion mutants (F) in HeLa cells.

(E) Schematic representation of Reg1.

(G) Luciferase activity of HeLa cells transfected with indicated reporter and Reg1 mutant plasmids. Data are mean ± SD (n = 3).

See also Table S5.

Figure 6. UPF1 is essential for Reg1-mediated mRNA decay

(A and B) Reg1-mediated degradation of *Il6* was measured in UPF1 knockdown cells (A) and the autoradiographs were quantified (B).

(C) Luciferase activity of HeLa cells transfected with UPF1, UPF2 or UPF3x siRNA, indicated reporter and Reg1 expression plasmids.

(D) Luciferase activity of UPF1 knockdown HeLa cells transfected with indicated reporter and the Roquin-1 expression plasmid.

(E) HeLa cells were transfected with the indicated siRNA and stimulated with IL-1β. RNA expression profiles were analyzed by RT-qPCR.

(F) Cells expressing *Il6* were transfected with UPF1 siRNA and/or Flag-Reg1. *Il6* co-precipitated with Reg1 were analyzed by RT-qPCR.

(G) Tethering Reg1 did not destabilize the luciferase-5BoxB under knockdown of UPF1.

Luciferase activity of UPF1 knockdown HeLa cells transfected with indicated reporter and expression plasmids.

(H) Degradation of Il6CDS-5BoxB mRNA under treatment with anisomycin was measured and quantified.

(I) Immunoblot analysis of UPF1 co-precipitated with Flag-Reg1 in HeLa cells under treatment with anisomycin.

(J-L) HeLa cells transfected with UPF1 siRNA were reconstituted with siRNA-resistant HA-UPF1-WT^{R} or HA-UPF1-DEAA^{R}. Immunoblot analysis for the UPF1 reconstitution (J). Luciferase activity of reconstituted cells, after transfection of indicated reporter and Reg1 expression plasmids (K). RNA expression profiles of reconstituted cells stimulated with IL-1β (L).

Unless otherwise indicated, Data are mean ± SD (n = 3). See also Figure S6.

Figure 7. Roles of Reg1 and Roquin in the control of inflammatory mRNAs in response to LPS

(A-C) WT, *Reg1*$^{-/-}$ and *Roquin*$^{san/san}$ BMMs were stimulated with LPS. RNA expression profiles were analyzed by RT-qPCR (A). Ptgs2 expression were analyzed by immunoblotting (B). The Protein/mRNA ratio of Ptgs2 is shown in (C).

(D) WT, *Reg1*$^{-/-}$; *Roquin*$^{san/san}$, *Reg1*$^{-/-}$ and *Roquin*$^{san/san}$ MEFs were stimulated with LPS and RNA expression profiles were analyzed by RT-qPCR.

(E) GSEA of overlap between Reg1 (left) or Roquin (right) target genes (RIP-seq based) and *Reg1*$^{-/-}$; *Roquin*$^{San/San}$ enrichment (transcriptome analysis based). An ES plot is shown with genes ranked according to their *Reg1*$^{-/-}$; *Roquin*$^{San/San}$ enrichment p value.

(F) GSEA of overlap between Reg1 (left) or Roquin (right) target genes (RIP-seq based) and *Reg1*$^{-/-}$ enrichment (transcriptome analysis based). An ES plot is shown with genes ranked according to their *Reg1*$^{-/-}$ enrichment p value.

(G) A proposed model of mRNA degradation by Reg1 and Roquin.

Unless otherwise indicated, Data are mean ± SD (n = 3). See also Figure S7 and Table S6.

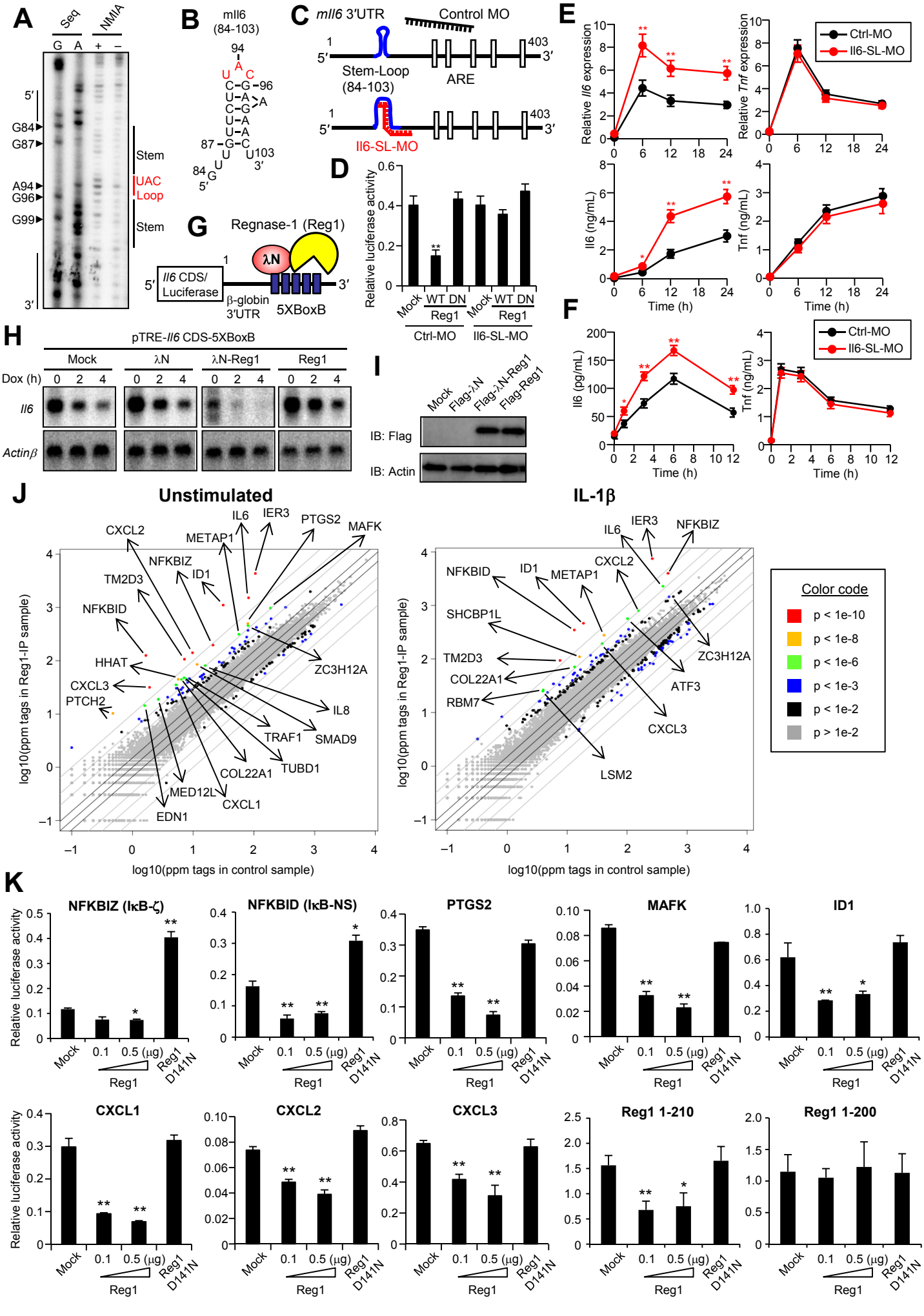
A
Seq
NMIA
G A + –
5′
G84
G87
A94
G96
G99
3′
Stem
UAC Loop
Stem
B
mIl6 (84-103)
94
U A C
C-G -96
U-A
C-G
U-A
U-A
87 -G-C
U U103
84 G U 3′
5′
C
mIl6 3′UTR
Control MO
1
403
5′
3′
Stem-Loop (84-103)
ARE
Il6-SL-MO
D
Relative luciferase activity
Mock
WT DN Reg1
Ctrl-MO
Il6-SL-MO
E
Relative Il6 expression
Relative Tnf expression
Ctrl-MO
Il6-SL-MO
Il6 (ng/mL)
Tnf (ng/mL)
Time (h)
F
Il6 (pg/mL)
Tnf (ng/mL)
Time (h)
G
Regnase-1 (Reg1)
λN
Il6 CDS/ Luciferase
β-globin 3′UTR
5XBoxB
H
pTRE-Il6 CDS-5XBoxB
Mock
λN
λN-Reg1
Reg1
Dox (h) 0 2 4
Il6
Actinβ
I
Mock
Flag-λN
Flag-λN-Reg1
Flag-Reg1
IB: Flag
IB: Actin
J
Unstimulated
IL-1β
log10(ppm tags in Reg1-IP sample)
log10(ppm tags in control sample)
CXCL2
METAP1
IL6
IER3
PTGS2
MAFK
NFKBIZ
ID1
TM2D3
NFKBID
HHAT
CXCL3
PTCH2
ZC3H12A
IL8
TRAF1
SMAD9
TUBD1
COL22A1
MED12L
CXCL1
EDN1
SHCBP1L
COL22A1
RBM7
ATF3
CXCL3
LSM2
Color code
p < 1e-10
p < 1e-8
p < 1e-6
p < 1e-3
p < 1e-2
p > 1e-2
K
NFKBIZ (IκB-ζ)
NFKBID (IκB-NS)
PTGS2
MAFK
ID1
CXCL1
CXCL2
CXCL3
Reg1 1-210
Reg1 1-200
Relative luciferase activity
Mock
0.1
0.5 (μg)
Reg1
Reg1 D141N

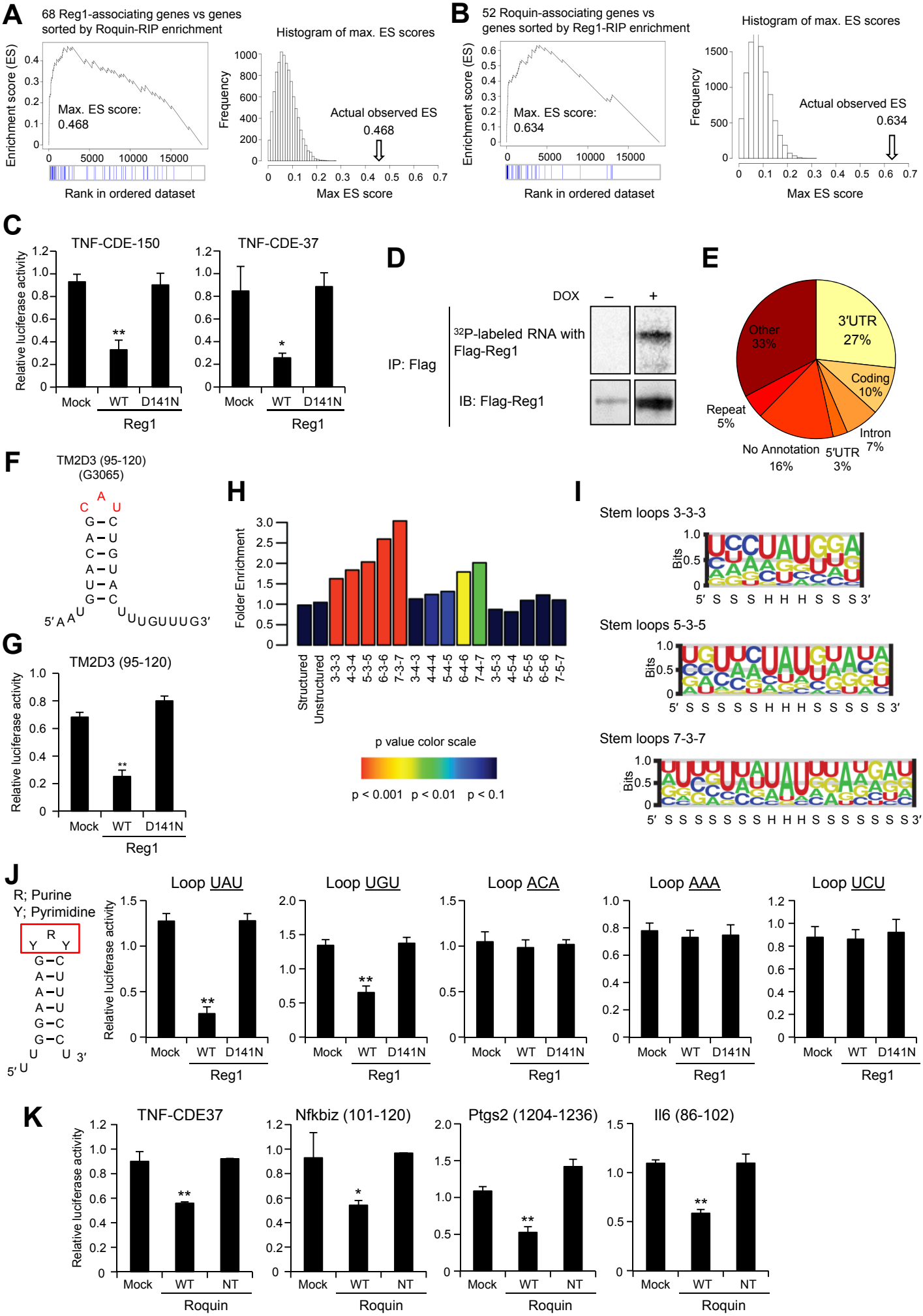
A
68 Reg1-associating genes vs genes sorted by Roquin-RIP enrichment
Enrichment score (ES)
Max. ES score: 0.468
Rank in ordered dataset
Histogram of max. ES scores
Frequency
Actual observed ES 0.468
Max ES score
B
52 Roquin-associating genes vs genes sorted by Reg1-RIP enrichment
Max. ES score: 0.634
Actual observed ES 0.634
C
TNF-CDE-150
TNF-CDE-37
Relative luciferase activity
Mock
WT
D141N
Reg1
D
DOX
IP: Flag
32P-labeled RNA with Flag-Reg1
IB: Flag-Reg1
E
3′UTR 27%
Coding 10%
Intron 7%
5′UTR 3%
No Annotation 16%
Repeat 5%
Other 33%
F
TM2D3 (95-120) (G3065)
5′ A A U U U G U U U G 3′
G
TM2D3 (95-120)
H
Folder Enrichment
Structured
Unstructured
3-3-3
4-3-4
5-3-5
6-3-6
7-3-7
3-4-3
4-4-4
5-4-5
6-4-6
7-4-7
3-5-3
4-5-4
5-5-5
6-5-6
7-5-7
p value color scale
p < 0.001 p < 0.01 p < 0.1
I
Stem loops 3-3-3
Stem loops 5-3-5
Stem loops 7-3-7
Bits
J
R; Purine
Y; Pyrimidine
5′ U U U 3′
Loop UAU
Loop UGU
Loop ACA
Loop AAA
Loop UCU
K
TNF-CDE37
Nfkbiz (101-120)
Ptgs2 (1204-1236)
Il6 (86-102)
Mock
WT
NT
Roquin

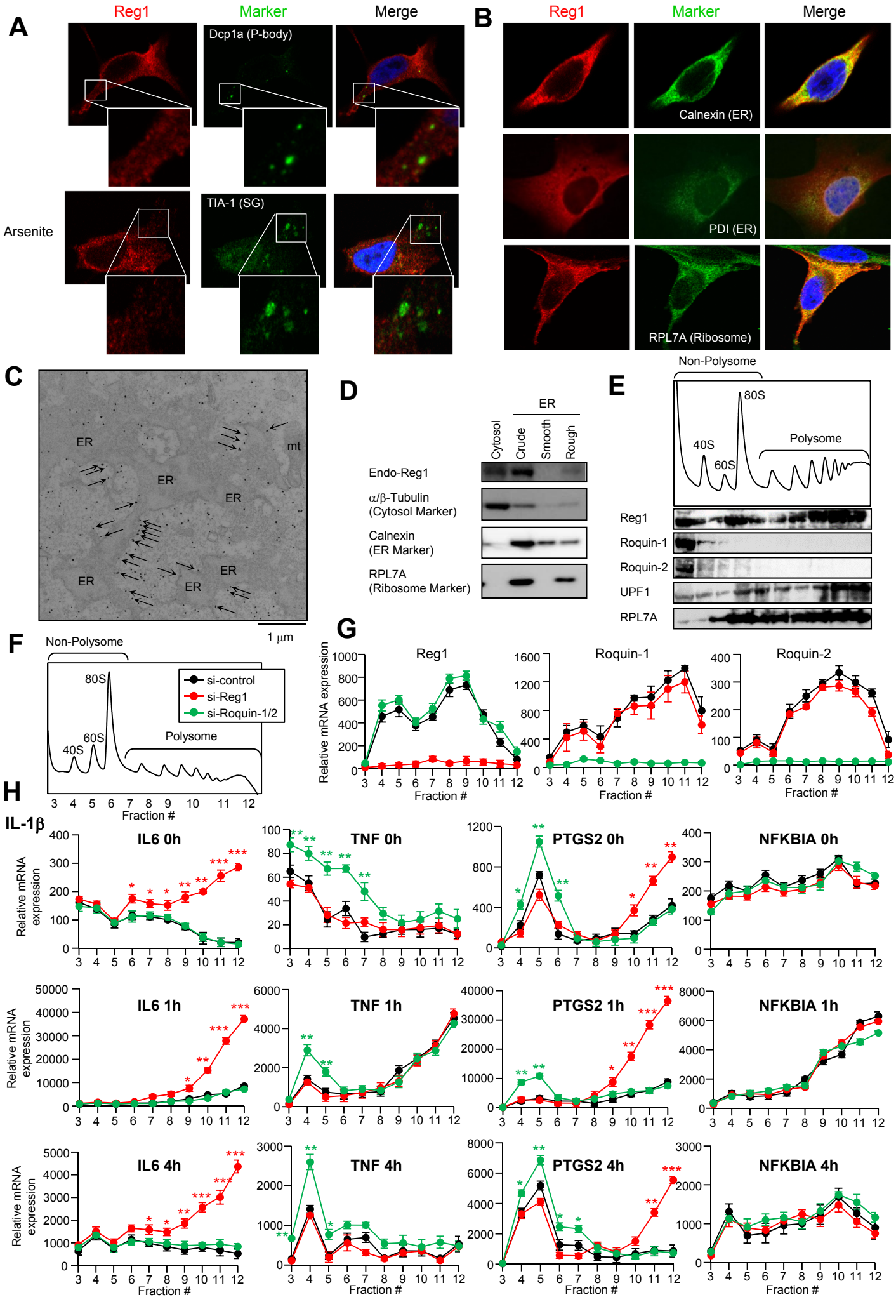
A
Reg1
Marker
Merge
Dcp1a (P-body)
Arsenite
TIA-1 (SG)
B
Reg1
Marker
Merge
Calnexin (ER)
PDI (ER)
RPL7A (Ribosome)
C
ER
mt
1 μm
D
ER
Cytosol
Crude
Smooth
Rough
Endo-Reg1
α/β-Tubulin
(Cytosol Marker)
Calnexin
(ER Marker)
RPL7A
(Ribosome Marker)
E
Non-Polysome
80S
40S
60S
Polysome
Reg1
Roquin-1
Roquin-2
UPF1
RPL7A
F
Non-Polysome
80S
60S
40S
Polysome
si-control
si-Reg1
si-Roquin-1/2
Fraction #
G
Reg1
Roquin-1
Roquin-2
Relative mRNA expression
Fraction #
H
IL-1β
IL6 0h
TNF 0h
PTGS2 0h
NFKBIA 0h
IL6 1h
TNF 1h
PTGS2 1h
NFKBIA 1h
IL6 4h
TNF 4h
PTGS2 4h
NFKBIA 4h
Relative mRNA expression
Fraction #

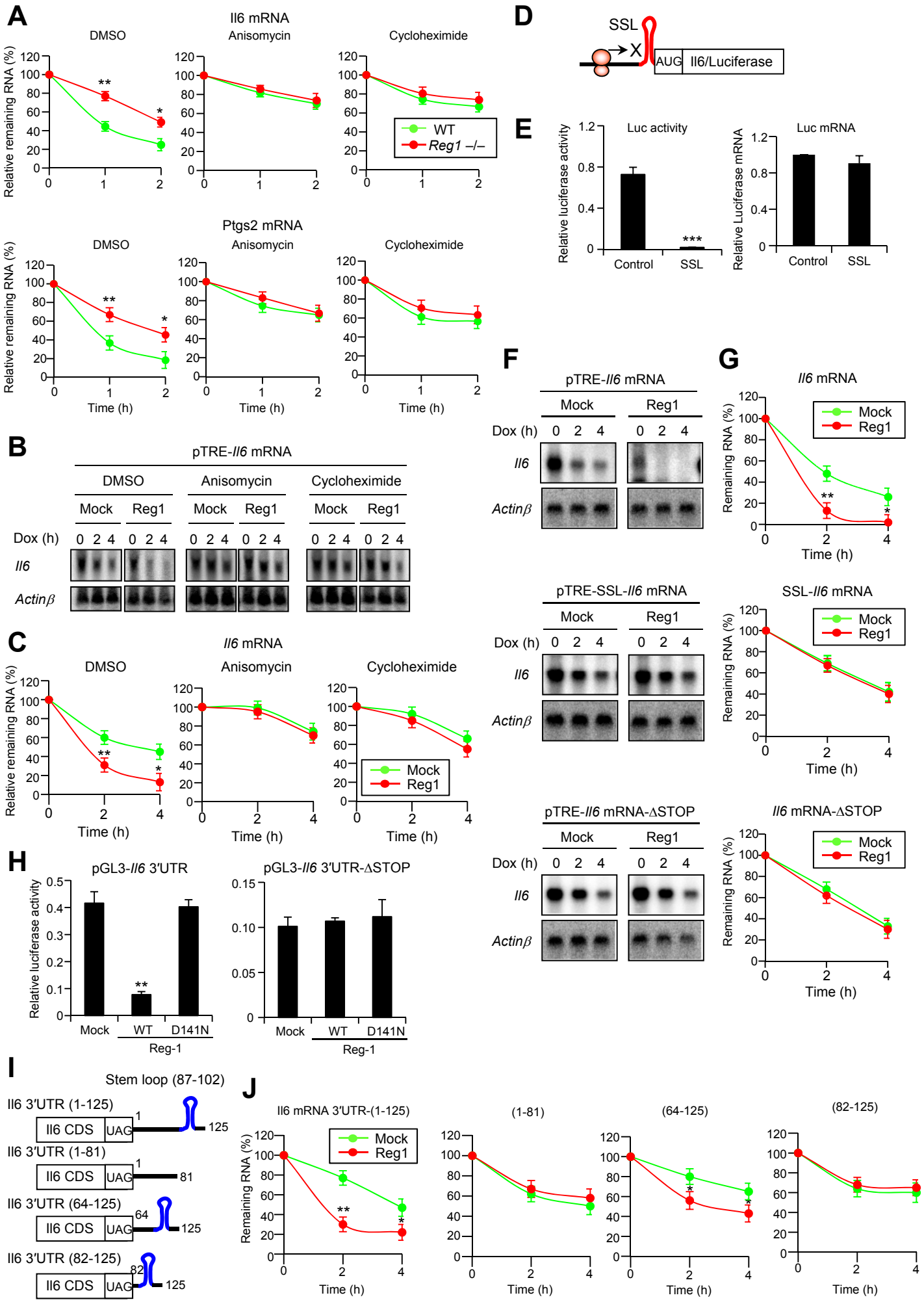
A
Il6 mRNA
DMSO
Anisomycin
Cycloheximide
Relative remaining RNA (%)
WT
Reg1 –/–
Ptgs2 mRNA
Time (h)
B
pTRE-Il6 mRNA
Mock
Reg1
Dox (h)
Il6
Actinβ
C
Il6 mRNA
D
SSL
X
AUG
Il6/Luciferase
E
Luc activity
Relative luciferase activity
Control
SSL
Luc mRNA
Relative Luciferase mRNA
F
pTRE-Il6 mRNA
pTRE-SSL-Il6 mRNA
pTRE-Il6 mRNA-ΔSTOP
G
Il6 mRNA
SSL-Il6 mRNA
Il6 mRNA-ΔSTOP
Remaining RNA (%)
H
pGL3-Il6 3′UTR
pGL3-Il6 3′UTR-ΔSTOP
Relative luciferase activity
Mock
WT
D141N
Reg-1
I
Stem loop (87-102)
Il6 3′UTR (1-125)
Il6 3′UTR (1-81)
Il6 3′UTR (64-125)
Il6 3′UTR (82-125)
Il6 CDS
UAG
J
Il6 mRNA 3′UTR-(1-125)
(1-81)
(64-125)
(82-125)

A

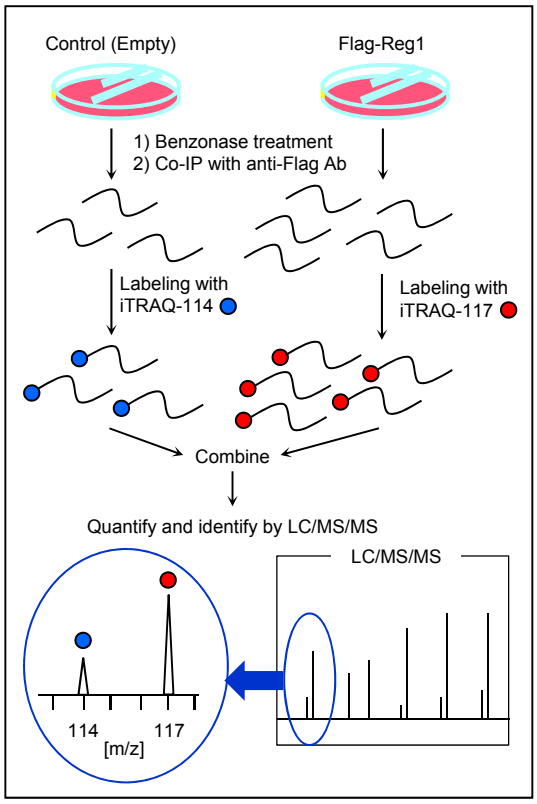

B

Accession No.	Protein Name	Fold Change (117/114)	117/114 Variability [%]
Q5D1E8	Zinc finger CCCH domain-containing protein 12A (ZC3H12A)	7.884	19.8
P07437	Tubulin beta chain (TUBB)	2.359	12.6
P62899	60S ribosomal protein L31(RPL31)	2.245	7.5
P46782	40S ribosomal protein S5 (RPS5)	1.825	13.5
P62701	40S ribosomal protein S4, X isoform (RPS4X)	1.741	6.8
P68104	Elongation factor 1-alpha 1 (EEF1A1)	1.724	10.8
P98175	RNA-binding protein 10 (RBM10)	1.635	1.3
P23246	Splicing factor, proline- and glutamine-rich (SFPQ)	1.534	0.7
P05387	60S acidic ribosomal protein P2 (RPLP2)	1.500	9.7
Q8NC51	Plasminogen activator inhibitor 1 RNA-binding protein (SERBP1)	1.413	18.8
P21333	Filamin-A (FLNA)	1.357	8.8
P63173	60S ribosomal protein L38 (RPL38)	1.341	12.4
P08708	40S ribosomal protein S17 (RPS17)	1.334	7.8
P55072	Transitional endoplasmic reticulum ATPase (VCP)	1.300	0.8
P24534	Elongation factor 1-beta (EEF1B2)	1.290	12.2
Q92900	UPF1 regulator of nonsense transcripts homolog (UPF1)	1.285	11.8
P35268	60S ribosomal protein L22 (RPL22)	1.270	4.4
P61978	Heterogeneous nuclear ribonucleoprotein K (HNRNPK)	1.262	4.3
Q9BUA3	Uncharacterized protein C11orf84 (C11orf84)	1.245	0.2
P62081	40S ribosomal protein S7 (RPS7)	1.233	7.0

C

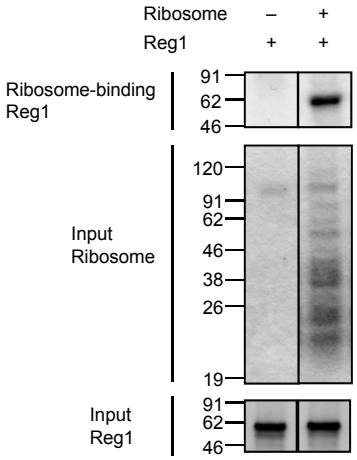

D

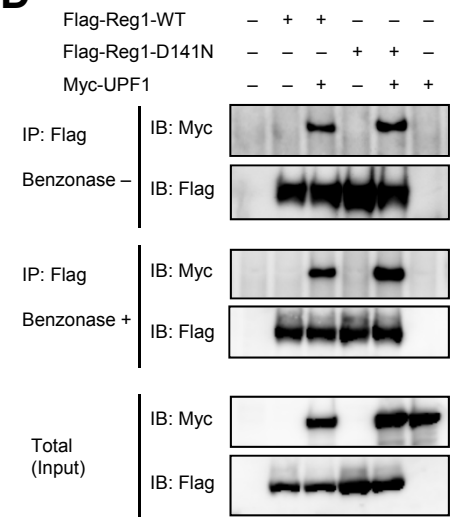

F

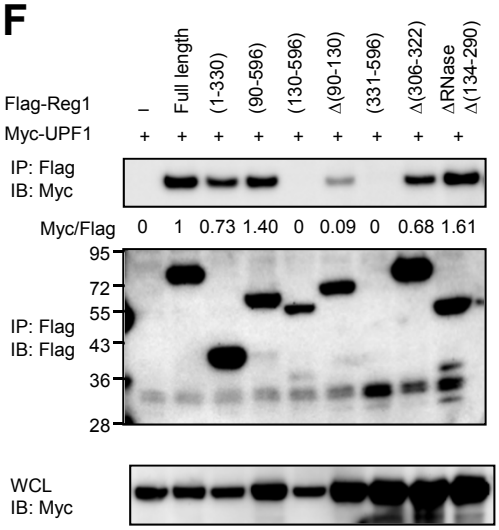

E

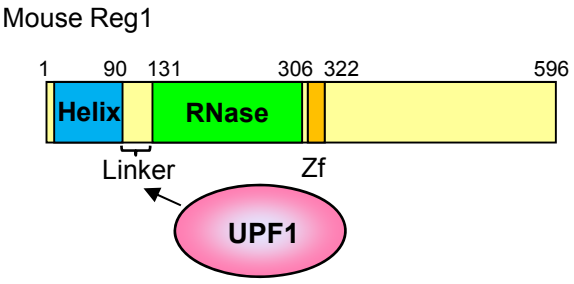

G

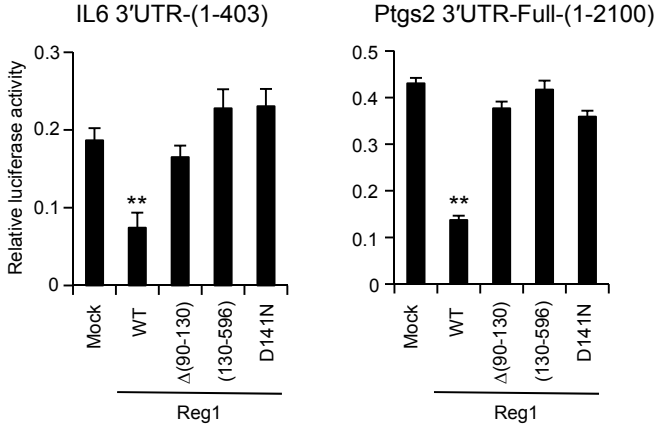

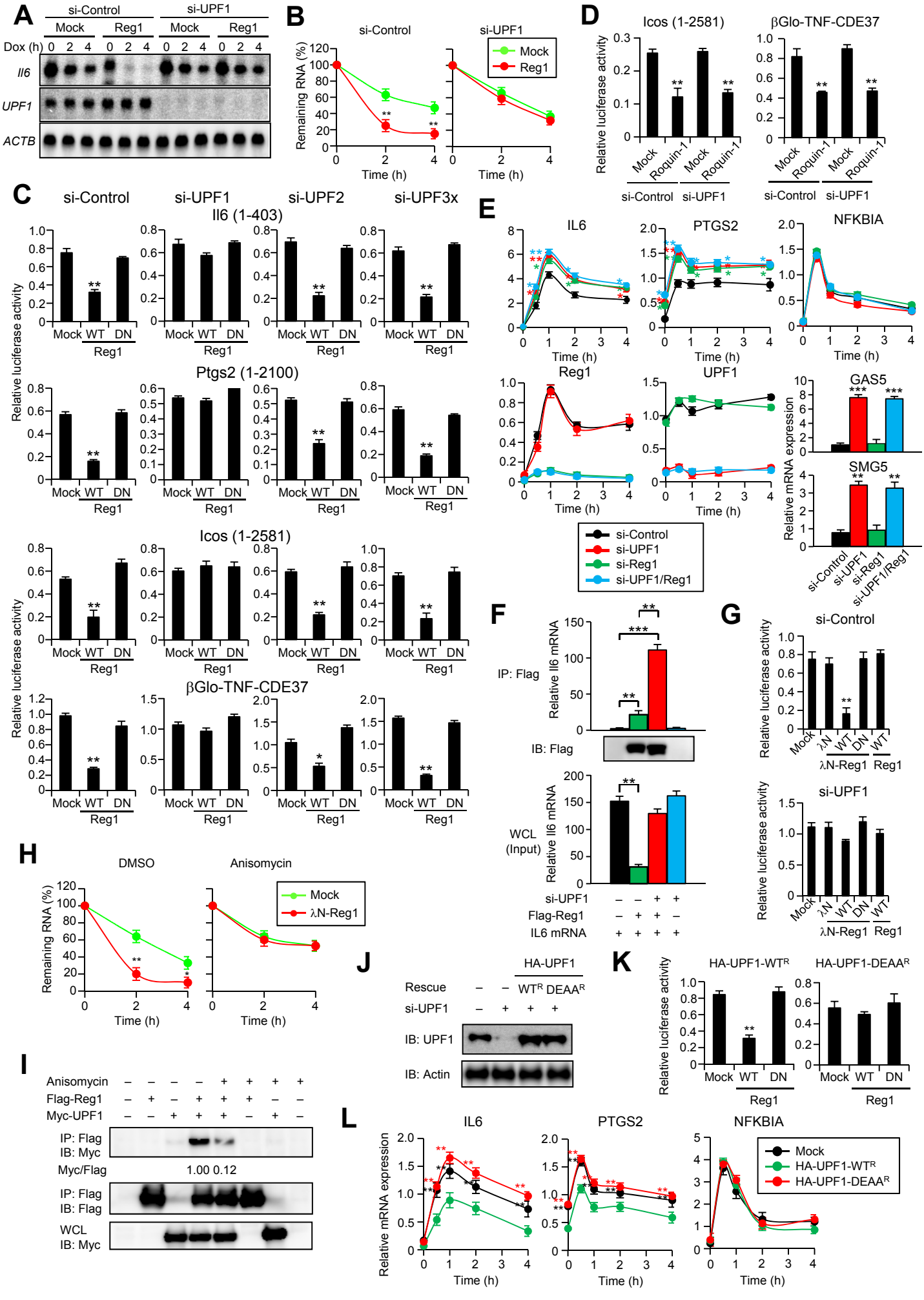
A
si-Control
si-UPF1
Mock
Reg1
Dox (h) 0 2 4 0 2 4 0 2 4 0 2 4
Il6
UPF1
ACTB
B
si-Control
si-UPF1
Mock
Reg1
Remaining RNA (%)
Time (h)
C
si-Control
si-UPF1
si-UPF2
si-UPF3x
Il6 (1-403)
Ptgs2 (1-2100)
Icos (1-2581)
βGlo-TNF-CDE37
Relative luciferase activity
Mock WT DN
Reg1
D
Icos (1-2581)
βGlo-TNF-CDE37
Relative luciferase activity
Mock
Roquin-1
si-Control
si-UPF1
E
IL6
PTGS2
NFKBIA
Reg1
UPF1
GAS5
SMG5
Time (h)
Relative mRNA expression
si-Control
si-UPF1
si-Reg1
si-UPF1/Reg1
F
IP: Flag
Relative Il6 mRNA
IB: Flag
WCL (Input)
si-UPF1
Flag-Reg1
IL6 mRNA
G
si-Control
si-UPF1
Relative luciferase activity
Mock λN WT DN WT
λN-Reg1
Reg1
H
DMSO
Anisomycin
Mock
λN-Reg1
Remaining RNA (%)
Time (h)
I
Anisomycin
Flag-Reg1
Myc-UPF1
IP: Flag
IB: Myc
Myc/Flag
1.00 0.12
IP: Flag
IB: Flag
WCL
IB: Myc
J
HA-UPF1
Rescue
si-UPF1
WTR DEAAR
IB: UPF1
IB: Actin
K
HA-UPF1-WTR
HA-UPF1-DEAAR
Relative luciferase activity
Mock WT DN
Reg1
L
IL6
PTGS2
NFKBIA
Relative mRNA expression
Time (h)
Mock
HA-UPF1-WTR
HA-UPF1-DEAAR

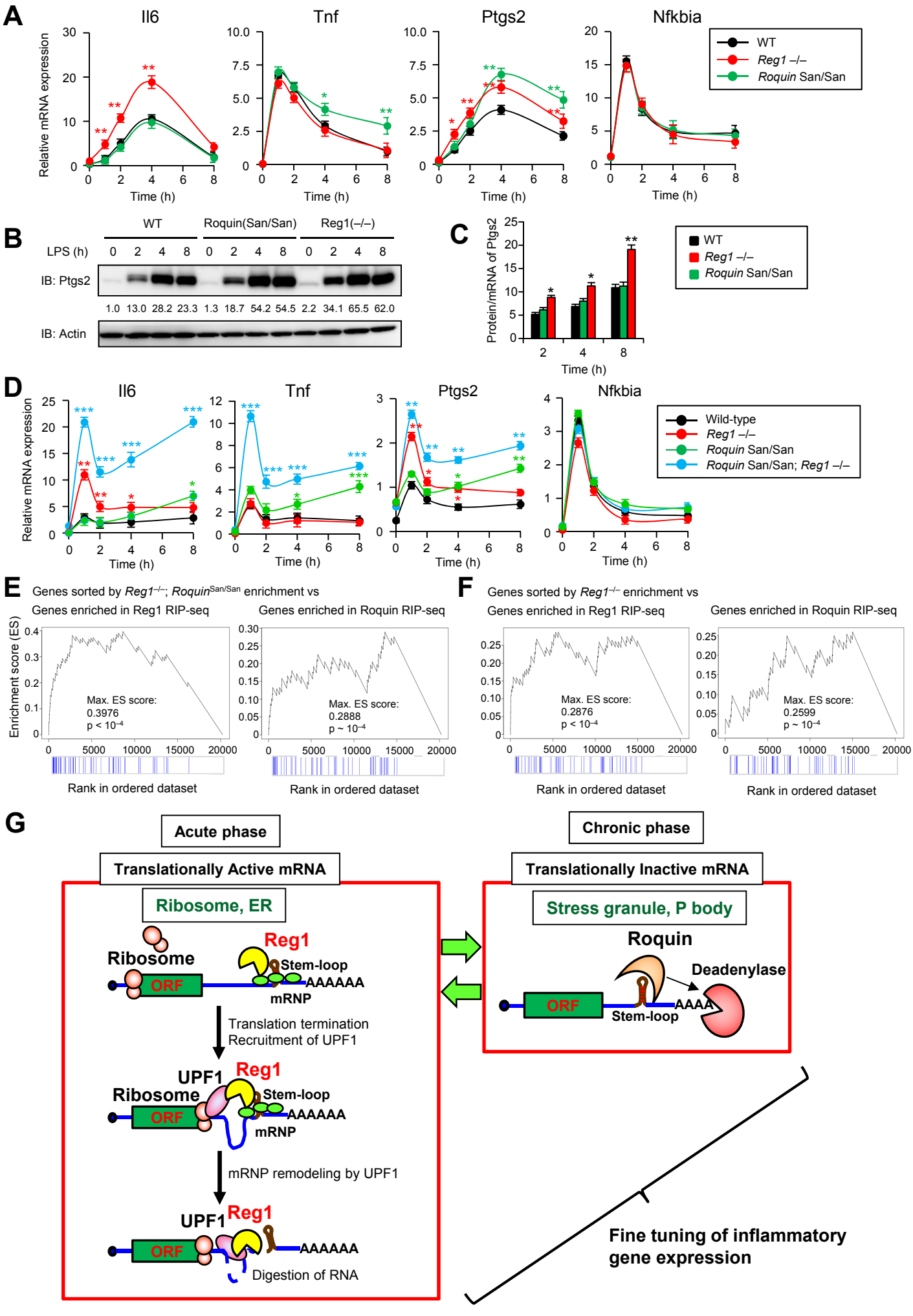
A
Il6
Tnf
Ptgs2
Nfkbia
Relative mRNA expression
Time (h)
WT
Reg1 –/–
Roquin San/San
B
WT
Roquin(San/San)
Reg1(–/–)
LPS (h)
IB: Ptgs2
1.0 13.0 28.2 23.3 1.3 18.7 54.2 54.5 2.2 34.1 65.5 62.0
IB: Actin
C
Protein/mRNA of Ptgs2
Time (h)
WT
Reg1 –/–
Roquin San/San
D
Il6
Tnf
Ptgs2
Nfkbia
Relative mRNA expression
Time (h)
Wild-type
Reg1 –/–
Roquin San/San
Roquin San/San; Reg1 –/–
E
Genes sorted by Reg1–/–; RoquinSan/San enrichment vs
Genes enriched in Reg1 RIP-seq
Genes enriched in Roquin RIP-seq
Enrichment score (ES)
Max. ES score: 0.3976
p < 10–4
Max. ES score: 0.2888
p ~ 10–4
Rank in ordered dataset
F
Genes sorted by Reg1–/– enrichment vs
Genes enriched in Reg1 RIP-seq
Genes enriched in Roquin RIP-seq
Max. ES score: 0.2876
p < 10–4
Max. ES score: 0.2599
p ~ 10–4
Rank in ordered dataset
G
Acute phase
Translationally Active mRNA
Ribosome, ER
Ribosome
Reg1
ORF
Stem-loop
AAAAAA
mRNP
Translation termination
Recruitment of UPF1
UPF1
mRNP remodeling by UPF1
Digestion of RNA
Chronic phase
Translationally Inactive mRNA
Stress granule, P body
Roquin
Deadenylase
AAAA
Fine tuning of inflammatory gene expression

Extended Experimental Procedures

Mice

Mice deficient in Reg1 have been described (Matsushita et al., 2009). *Sanroque* mice were kindly provided by Dr. Masakazu Hattori (Kyoto University). *Il6*$^{-/-}$ mice were kindly provided by Dr. Masao Matsuoka (Kyoto University). All animal experiments were done with the approval of the Animal Research Committee of the Institute for Virus Research, Kyoto University.

Cell culture and transfection

Primary MEFs were prepared from wild-type, *Reg1*$^{-/-}$, *Roquin*$^{san/san}$ or *Reg1*$^{-/-}$/*Roquin*$^{san/san}$ mouse embryos at embryonic day 13.5. Dicer-ablated MEFs were provided by Stephen N. Jones (Mudhasani et al., 2008). MEFs, NIH3T3 cells, RAW cells, HeLa cells and HEK293 cells were maintained in DMEM (Nacalai Tesque) supplemented with 10% (vol/vol) FBS and 50 μM β-mercaptoethanol (Invitrogen). Tet-off HEK293 cells were purchased from Clontech and maintained in α-MEM (Nacalai Tesque) supplemented with 10% (vol/vol) FBS (Clontech), 50 μM β-mercaptoethanol and 100 μg/mL G418 (Nacalai Tesque). Flp-In 293 T-REx cells (Invitrogen) were grown in DMEM high glucose with 10% (v/v) FBS and 2 mM L-glutamine. Cells were transfected through the use of Lipofectamine 2000, Lipofectamine 3000, Lipofectamine LTX (Invitrogen), the Neon transfection system (Invitrogen) or the Nucleofector system (Lonza) according to the manufacturer's recommendations.

For siRNA-mediated knockdown, cells were transfected through the use of Lipofectamine RNAiMAX (Invitrogen), MISSION siRNA Transfection Reagent (Sigma) or the Neon transfection system (Invitrogen). The siRNAs used in this study were synthesized by Ambion and the following siRNA target sequences were used: hUPF1, 5′-GAUGCAGUUCCGCUCCAUUdTdT-3′; mUPF1,

5'-CAGUUACUGUGGAAUCCAUdTdT-3'; hUPF2,

5′-GGCUUUUGUCCCAGCCAUCdTdT-3′; mUPF2,

5'-GCAAGCUUCUGUACAAGGAdTdT-3'; hUPF3x,

5′-GGAGAAGCGAGUAACCCUGdTdT-3′; mUPF3x,

5'-CUAUCGAGGAUGAUCCAGAdTdT-3'; hRoquin-1,

5′-GAUCGAGAGUUACUAUCCAdTdT-3′; hRoquin-2,

5′-GCUUGAAAAGUAUCGAUUAdTdT-3′; mRoquin-1,

5′-CGCACAGUUACAGAGCUCAdTdT-3′; mRoquin-2,

5′-GGACUUGGCUCAUAAAUCAdTdT-3′; hReg1,

5′-GUGUCCCUAUGGAAGGAAAdTdT-3′; mReg1,

5′-CAACUUCCUUCGUAAGAAAdTdT-3′; hSTAU1,

5'-GGACUAGUAAUAAAGAGGAdTdT-3'; mStau1,

5'-GAUUUUCCCAAGAACAACAdTdT-3'.

Peritoneal macrophages were prepared from mice 3 d after intraperitoneal injection of 4% (vol/vol) thioglycollate medium (2 ml) (Sigma) and were maintained in RPMI-1640 medium (Nacalai Tesque) supplemented with 10% (vol/vol) FBS and 50 μM β-mercaptoethanol.

For preparation of bone marrow–derived macrophages (BMMs), bone marrow cells were isolated from wild-type, *Reg1*$^{-/-}$, or *Roquin*$^{san/san}$ mice and cultured in macrophage growth medium (RPMI-1640 medium supplemented with 10% (vol/vol) FBS, 50 μM β-mercaptoethanol, 100 U/ml of penicillin, 100 μg/ml of streptomycin and 20 ng/ml of macrophage colony-stimulating factor). After 5 days, cells were washed once and cultivated for 2 days with macrophage growth medium, then cells were collected for further analysis.

Plasmid construction and reagents

The cDNAs of mouse Reg1 (Zc3h12a), the D141N mutant and mouse Il6 have been

described (Matsushita et al., 2009). The cDNAs of Reg1 were ligated to the vector pFlag-CMV2 (SIGMA) and pcDNA3.1(+) (Invitrogen) for mammalian expression, pMRX-ires-puro (Cell Biolabs) for retrovirus production, pGEX-6P1 (GE Healthcare) for *E. coli* expression and pTNT vector (Promega) for protein production. The cDNAs of Il6 CDS-3′ UTR and β-globin CDS-Reg1 3′ UTR were inserted in pTREtight vector (Clontech). The 3′ UTR cDNAs of Il6 were inserted downstream of the T7 promoter of pBluescript II KS (–) (Stratagene). The 3′ UTR cDNAs of a set of genes were inserted in the pGL3-promoter (Promega). pENTR4 constructs were generated by PCR amplification of the Reg1 coding sequences (CDS) from cDNA followed by restriction digest and ligation into the pENTR4 (Invitrogen) backbone, which were further recombined into the pFRT/TO/FLAG/HA-DEST destination vector (Baltz et al., 2012) using GATEWAY LR recombinase (Invitrogen) according to manufacturer's protocol.

TOPuro-hCaf1a-AA-mycSG, pcDNA3-Flag-hDcp2-AA, pLNCX2-EGFP-mRoquin, and pCI-neo-Flag-mRoquin were kindly provided by Georg Stoecklin (German Cancer Research Center). pSR-myc-hUPF1-WT, siRNA-resistant pSR-HA-hUPF1-WT(R) and pSR-HA-hUPF1-D648A/E649A (DEAA) (R) were kindly provided by Akio Yamashita (Yokohama City University).

LPS from Salmonella minnesota and puromycin were from Invivogen. Recombinant cytokines were from R&D Systems. Anisomycin, cycloheximide and actinomycin D were from Sigma; Harringtonine was from LKT Laboratories.

In vitro RNA cleavage assay

In vitro RNA cleavage assay has been previously described (Matsushita et al., 2009). Briefly, Recombinant Reg1 protein (Matsushita et al., 2009) and in vitro transcribed 5′-[^{32}P]-labelled RNAs were mixed in cleavage buffer (25 mM HEPES, 50 mM potassium acetate, 5 mM DTT, 5 mM magnesium acetate and 0.2 U/ml RNasin (Promega)). The cleaved RNA was purified with Trizol (Invitrogen) and analysed by

denaturing 6% polyacrylamide-TBE-urea gels (Invitrogen) and autoradiography.

For generation of the circular RNA, in vitro transcribed 5′-[^{32}P]-labelled mIl6 3′ UTR (1-403) RNA was circularised by T4 RNA Ligase 1 (ssRNA Ligase) (NEB) in ligation buffer (50 mM Tris-HCl, pH 7.5, 10 mM $MgCl_2$, 1 mM DTT, 10% PEG_{8000}, 50 μM ATP and 0.2 U/ml RNasin (Promega)) at 25ºC for 2 h. The RNA product was subjected to in vitro RNA cleavage assay as described above.

RNA motif exploring by selective 2′-hydroxyl acylation analyzed by primer extension (SHAPE) chemistry and computational analysis

RNA SHAPE chemistry has been described (Wilkinson et al., 2006). Briefly, DNA templates for mIl6 3′ UTR (84-103), mPtgs2 3′ UTR (1204-1237) or stem-loop structure were inserted in the context of flanking 5′ and 3′ structure cassette (Wilkinson et al., 2006), which was inserted downstream of the T7 promoter of pBluescript II KS (–) (Stratagene), and in vitro transcribed by T7 RNA polymerase (MEGAscript T7 Transcription Kit, Invitrogen). The in vitro transcribed RNAs were refolded in RNA folding buffer (100 mM Tris-HCl, pH 8.0, 100 mM NaCl and 6 mM $MgCl_2$) in a final volume of 18 μl. After folding, RNAs were modified in the presence of 6.5 mM N-methylisatoic anhydride (NMIA) (M-25; Invitrogen) and incubated at 20ºC for 4 h. After modification, RNAs were subjected to reverse transcription (ReverTra Ace, Toyobo) using a 5′-[^{32}P]-labelled DNA primer (5′-GAACCGGACCGAAGCCCG-3′) specific to the 3′ structure cassette. For G or A sequencing experiment, primer extensions were performed in the presence of cytosine or thymidine dideoxy terminating nucleotides, respectively. The cDNA fragments are resolved on denaturing 8% polyacrylamide-TBE-urea sequencing gels followed by autoradiography. Computational prediction of the RNA secondary structures was performed using the RNAfold from the Vienna package (Lorenz et al., 2011).

Tethered Function Assays

Reg1 was artificially recruited to reporter mRNAs by the BoxB-λN-peptide tethering system (Mishima et al., 2012). The 22 amino acid RNA-binding domain of λN peptide was fused with the N terminus of Reg1 and five 19 nt λN binding sequences (5XBoxB) were tandemly inserted in a downstream of Il6 coding sequence (CDS) or luciferase CDS. Tet-off 293 cells and HeLa cells were transfected with the 5XBoxB reporter plasmids, together with expression plasmid for Flag-λN-Reg1 or empty (control) plasmid followed by luciferase assay, mRNA decay assay and RNA IP.

RNA immunoprecipitations (RIP)-sequencing analysis

RNA immunoprecipitation was performed using a RIP-Assay Kit (RN1001; Medical & Biological Laboratories) according to the manufacturer's protocol with some modifications. Briefly, HeLa cells were transfected with expression vector for Flag-tagged Reg1-D141N mutant, Roquin-1 or empty (control) vector and stimulated with IL-1β (10 ng/mL) for 0 or 2 h. RNA-protein complexes from lysate of HeLa cells were immunoprecipitated with anti-Flag antibody (F3165; Sigma) bound to protein G magnetic beads and RNAs were extracted from the beads. The quality of RNA was analyzed by the Bioanalyzer Nano 6000 chip (Agilent Technologies). Only samples with an RNA Integrity Number (RIN) greater than 9.0 were used for further experiments. RNA library was prepared using Small RNA Sample Prep kit v1.0 (Illumina Inc.) and sequenced on a HiSeq 2000 system (Illumina) also according to the manufacturer's instructions. Fourteen and 0.6 million RNA reads were obtained for Reg1 and 16.1 million for control. The resulting set of trimmed reads were then mapped against the human genome (hg19; NCBI). Analysis of enrichment of mapped reads in the Reg1 RIP samples vs control IP samples was performed using the R package DESeq (Anders and Huber, 2010), as follows. The count of mapped reads to each gene was used as input for the method. The coverage of each sample and the dispersions were estimated from the

read count data using the functions provided in the package. Finally, differential tag counts for each gene between the RIP and control sample for each of the two time points were estimated based on the negative binomial distribution. Genes with an unadjusted p value for enrichment in the RIP samples ≤ 1e-3 were regarded as candidate Reg1 targets.

Analysis of overlap with between Reg1 targets and Roquin targets.

The overlap between the targets of Reg1 and those of Roquin was evaluated using three measures. First, we employed the Gene Set Enrichment Analysis (GSEA) methodology, as described (Subramanian et al., 2005). In this case, we defined a set of genes S as the Reg1 targets based on their enrichment in RIP-seq samples at 0h, 2h, and both time points combined. On the other hand, a ranked list L was obtained by sorting the genome-wide set of genes by their enrichment in the Roquin RIP-seq samples of the same time points. The distribution of S in L was evaluated by calculating an Enrichment Score (ES) and the estimation of a significance level for ES by 10,000 random permutations, as described (Subramanian et al., 2005). The P value of enrichment of S in the top of L was estimated as the fraction of permuted samples resulting in a higher ES than the actual data.

The statistical significance of overlap between Reg1 targets and Roquin targets was also evaluated using the Kolmogorov-Smirnov statistical test, which is closely related to the GSEA approach, and the hypergeometric distribution. In the latter case, Roquin targets were defined as the 52 genes having a p value of enrichment in the RIP sample smaller than 0.01 at either of the time points, and Reg1 targets as 68 genes having a p value of enrichment < 0.001 at either of the time points. The number of overlapping targets of both time points were compared to the expected number according to the hypergeometric distribution. Both the Kolmogorov-Smirnov and the hypergeometric test were performed using the R language. Candidate mouse Roquin targets were

obtained from (Leppek et al., 2013). The 92 human homologs of the mouse targets were defined using human-mouse homology data as available from the Mouse Genome Database (MGD) at the Mouse Genome Informatics website, The Jackson Laboratory (http://www.informatics.jax.org; April 2014).

Generation of NIH3T3 cells stably expressing Flag-tagged Reg1

NIH3T3 cells were transduced with retroviral supernatant for 12 h. Retroviral supernatants were produced by PlatE packaging cells (Cell Biolabs) transfected with retroviral expression vectors. Supernatants were collected 48 h after transfection, were filtered through 0.22-μm filters and were used for infection. After transduction, cells were washed and resuspended for 12 h in maintenance media. Cells were washed once and cultured in maintenance media with 2 μg/ml puromycin. Stable clones were obtained by selection in the presence of puromycin (2 μg/mL) and analyzed by Western blotting for the expression of Flag-tagged Reg1 using the anti-Flag antibody M2 (F3165; Sigma).

Fluorescence microscopy

For immunofluorescence staining, NIH3T3 cells stably-expressing Flag-tagged Reg1 were used because of large cell cytoplasm in this cell type. In addition, HeLa cells transiently-expressing Flag-tagged Reg1 were also used. The cells were fixed in 3% paraformaldehyde in PBS for 15 min, incubated with 50 mM NH_4Cl in PBS for 10 min, permeabilized in 0.5% Triton X-100 and 0.1% gelatin in PBS for 10 min, washed three times in 0.1% gelatin in PBS and blocked in 0.1% gelatin and 2% goat-serum (X0907; Dako) in PBS for 30 min at room temperature. Primary antibodies to Flag (F3165 or F7425; Sigma), α/β-Tubulin (#2148; Cell Signaling Technology), Calnexin (ab22595; Abcam), PDI (#3501; Cell Signaling Technology), RPL7A (15340-1-AP; Proteintech Group), Dcp1a (ab47811; Abcam) or TIA1 (ab40693; Abcam) were used for staining in

combination with secondary antibodies conjugated to Alexa 488 (A11017 or A11070; Invitrogen) or Alexa 568 (A11019 or A21069; Invitrogen). Images were captured on a Leica TCS SPE confocal microscopes (Leica) and an All-in-one Type Fluorescence Microscope (BZ-9000; Keyence) and analyzed with the LAS-AF software (Leica) and BZ Analyzer Software (Keyence), respectively.

For RNA fluorescence in situ hybridization (RNA FISH) combined with immunofluorescence (IF) staining, HeLa cells were stimulated with IL-1β (10 ng/ml) for 4 h and were subjected to RNA FISH. RNA FISH was performed using the RNAscope Multiplex Fluorescent Assay (Advanced Cell Diagnostics) according to the manufacturer's protocol with some modifications. Briefly, cells were fixed in 4% paraformaldehyde in PBS for 20 min, serially dehydrated and rehydrated for 5 min each in graded alcohol (50%, 70% and 100% EtOH), treated with protease for 10 min at room temperature and hybridized with RNAscope probes at 40°C. After the washing step, cells were blocked in 1% (wt/vol) Blocking Reagent (11096176001; Roche) in PBS for 1 h at room temperature. Primary antibodies to Dcp1a (ab47811; Abcam) were used for staining in combination with secondary antibodies conjugated to Alexa 568 (A21069; Invitrogen). Images were captured on a Leica TCS SPE confocal microscopes (Leica) and analyzed with the LAS-AF software (Leica).

Immunoelectron microscopy

Immunoelectron microscopy has been described (Matsunaga et al., 2009). Briefly, NIH3T3 cells stably-expressing Flag-tagged Reg1 were fixed with 4% paraformaldehyde for 30 min in 0.1 M sodium-phosphate buffer (pH 7.4) and washed for 5 min three times in the sodium-phosphate buffer. Cells were permeabilized and blocked for 30 min with 0.2% saponin, 10% BSA, 10% normal goat serum and 0.1% cold-water fish gelatin in the sodium-phosphate buffer. Cells were stained with anti-Flag mouse monoclonal antibody (F3165; Sigma) overnight at 4°C, washed for 10 min six

times in the sodium-phosphate buffer containing 0.1% saponin, then stained for 2 h at room temperature with an anti-mouse IgG conjugated to 1.4 nm gold particle (Nanogold Fab′ fragment of goat anti-mouse IgG) (2002; Nanoprobes), washing for 10 min five times in the sodium-phosphate buffer containing 0.1% saponin. Electron micrographs were obtained with a JEM-1011 transmission electron microscope (JEOL).

iTRAQ labeling and mass spectrometry

iTRAQ labeling was performed using an iTRAQ reagent kit (Applied Biosystems) according to the manufacturer's protocol with some modifications. Briefly, cell lysates from RAW cells stably expressing Flag-tagged Reg1 and HeLa cells transiently-expressing Flag-tagged Reg1 together with their controls (Empty) were immunoprecipitated with anti-Flag Ab in the presence of Benzonase (50 U/mL) (Novagen). The immunoprecipitaed proteins (5 μg each) were reduced, alkylated, digested, labeled with iTRAQ reagents and cleaned up with a cation exchange chromatography according to the manufacturer's (Applied Biosystems) protocol with some modifications. Control or Reg1 immunoprecipitates was labeled with iTRAQ Reagent 114 or 117, respectively. The iTRAQ reagent-labeled sample was analyzed by LC-MS/MS (Orbitrap LC-MS; Thermo Fisher Scientific). Proteins were identified by database searching using Mascot Daemon (Matrix Science). Based on an 80% confidence level (< 20% 117/114 variability), cutoff values of 1.2-fold for up-regulated proteins were used to define candidate proteins as Reg1-associated proteins.

Sucrose gradient centrifugation (polysome profiles)

HeLa cells were lysed in polysome buffer (20 mM HEPES-KOH [pH 7.5], 100 mM KCl, 5 mM $MgCl_2$, 0.25% (vol/vol) Nonidet P-40, 10 μg/ml cycloheximide, 100 units/ml RNase inhibitor, protease inhibitor cocktail). Lysates were loaded on top of a linear 15%–60% sucrose gradient (15%–60% sucrose, 20 mM HEPES-KOH [pH 7.5],

100 mM KCl, 5 mM $MgCl_2$, 10 μg/ml cycloheximide, 100 units/ml RNase inhibitor, protease inhibitor cocktail). After ultracentrifugation at 38,000 rpm for 2.5 h at 4ºC in a HITACHI P40ST rotor, fractions were collected from the top of the gradient and subjected to UV-densitometric analysis. The absorbance profiles of the gradients were determined at 254 nm. For disassociation of ribosome and polysome, EDTA was added to Mg^{2+}-free polysome buffer and 15%–60% sucrose gradient at concentrations of 50 mM and 20 mM, respectively. For protein analysis, each fraction was subjected to TCA precipitation and SDS-PAGE. Immunoblotting was performed using the indicated antibodies. For RNA analysis, each fraction was subjected to High Pure RNA Isolation Kit (Roche) and RT-qPCR.

Immunoblot analysis

Whole-cell extracts were prepared in lysis buffer (1% (vol/vol) Nonidet P-40, 0.1% (wt/vol) SDS, 1% (wt/vol) sodium deoxycholate, 150 mM NaCl, 20 mM Tris-HCl, pH 8.0, 10 mM EDTA and Complete Mini Protease Inhibitor Cocktail without EDTA (Roche)). The following antibodies were used for immunoblot analysis: antibody to Flag (F3165 and F7425; Sigma), c-Myc (M4439 and C3956; Sigma), α/β-Tubulin (#2148; Cell Signaling Technology), Calnexin (ab22595; Abcam), PDI (#3501; Cell Signaling Technology), Roquin-1 (A300-514A; Bethyl Laboratories, Inc.), Roquin-2 (ab99090; Abcam), Staufen1 (STAU1) (A303-956A; Bethyl Laboratories, Inc.), UPF2 (ab153830; Abcam), UPF3 (ab83249; Abcam), Dcp1a (ab47811; Abcam), TIA1 (ab40693; Abcam), RPL7A (15340-1-AP; Proteintech Group), RPS4X (14799-1-AP; Proteintech Group), RPL7 (ab72550; Abcam), Ptgs2 (ab15191; Abcam) and β-actin (sc-1615; Santa Cruz). Rabbit UPF1 antibody was kindly provided by Akio Yamashita (Yokohama City University). Rabbit Reg1 antibody has been described (Iwasaki et al., 2011). Luminescence was detected with a luminescent image analyzer (ImageQuant LAS 4000; GE Healthcare).

Subcellular fractionation

Subcellular fractionation was performed using an Endoplasmic Reticulum Isolation Kit (Sigma) following the manufacturer's instructions. Briefly, NIH3T3 cells were suspend in hypotonic extraction buffer (10 mM HEPES, pH 7.8, 25 mM potassium chloride and 1 mM EGTA) to allow the cells to swell. Cells were adjusted to isotonic conditions by the addition of isotonic extraction buffer (10 mM HEPES, pH 7.8, 250 mM sucrose, 25 mM potassium chloride and 1 mM EGTA) and homogenized by the Dounce homogenizer. The total lysate was centrifuged at 1,000 x g for 10 min at 4ºC, yielding a pellet consisting mainly of nuclei and unbroken cells. The supernatant was centrifuged at 12,000 x g for 15 min at 4ºC, yielding a pellet consisting mainly of mitochondria. The supernatant was ultracentrifuged at 100,000 x g for 1 h at 4ºC, yielding a pellet consisting mainly of microsomal fraction (cellular membranes, SER and RER). The supernatant from this 100,000 x g spin consists mostly of cytosol. The pellet consisting of microsomal fraction was resuspended in the isotonic extraction buffer and applied to an Optiprep gradient and ultracentrifuged at 150,000 x g for 3 h at 4ºC to obtain SER and RER fractions. Each fraction was collected and analyzed by Western blot with the indicated antibodies.

Recombinant Reg1 proteins

Flag-tagged Reg1 protein and its mutant protein were translated *in vitro* in the presence of [^{35}S]-methionine with the TNT-coupled reticulocyte lysate system (Promega) following the manufacturer's instructions with some modifications. After *in vitro* translation, lysates were treated with Benzonase (Novagen) and [^{35}S]-labeled proteins were affinity purified using anti-Flag antibody affinity resin (Sigma) and eluted with a 3 x Flag peptide (Sigma). The [^{35}S]-labeled proteins were characterized with quantitative autoradiography.

Ribosome-binding assay

Ribosomes were purified from HeLa cells by sedimentation through a sucrose cushion (Zinzalla et al., 2011). Recombinant [^{35}S]-radioactive Reg1 protein was incubated in ribosome binding buffer (10 mM Tris-HCl, pH 7.6, 100 mM KCl, 10 mM $MgCl_2$, 1 mM DTT, 0.1 mg/mL BSA) for 30 min at 4ºC in the simultaneous absence or presence of the highly-purified ribosome (5 μg). Subsequently the mixture was loaded on a 10% sucrose cushion (10 mM Tris-HCl, pH 7.6, 100 mM KCl, 10 mM $MgCl_2$, 10% (wt/vol) Sucrose) and ultracentrifuged for 20 min at 300,000 x g at 4ºC to pellet the ribosome and ribosome-associated protein. The pellets were analyzed by SDS-PAGE and quantitative autoradiography.

Quantitative PCR analysis

Total RNA was isolated using ISOGEN II (Wako) or Trizol (Invitrogen) and reverse-transcribed using ReverTra Ace (Toyobo) or MicroRNA RT Kit (Applied Biosystems) according to the manufacturer's instructions. For quantitative PCR, cDNA fragments were amplified through the use of Thunderbird Probe qPCR Mix (Toyobo) or TaqMan® MicroRNA Assays (Applied Biosystems); TaqMan probes for mouse Il6, mouse β-Actin, mouse 18S rRNA, human IL6, human 18S rRNA and human β-ACTIN were from Applied Biosystems. Fluorescence was detected with a StepOne Real-Time PCR System (Applied Biosystems). For analysis of the induction mRNA in response to LPS stimulation, the abundance of mRNA of each expressed gene was normalized to that of 18S rRNA or β-Actin.

Protein IP

HeLa cells and Tet-off 293 cells transiently-expressing Flag-tagged Reg1 and RAW cells and Jurkat cells stably-expressing Flag-tagged Reg1 were lysed in lysis buffer

(0.5% (vol/vol) Nonidet P-40, 150 mM NaCl, 10 mM Tris-HCl, pH 8.0 and Complete Mini Protease Inhibitor Cocktail without EDTA (Roche)). Anti-Flag antibody (F3165; Sigma) bound to protein G magnetic beads (Invitrogen) was incubated for 3 h at 4ºC with lysates. Beads were washed three times with lysis buffer and suspended in SDS sample buffer (50 mM Tris-HCl, pH 6.8, 2% (wt/vol) SDS, 5% (vol/vol) β-mercaptoethanol, 10% (vol/vol) glycerol and bromophenol blue). Samples were boiled for 5 min at 95°C and analyzed by Western blot with the indicated antibodies.

RNA IP

HeLa cells and Tet-off 293T cells transfected with the indicated siRNA and expression plasmids and RAW cells stably expressing Flag-tagged Reg1 were lysed in RNA IP lysis buffer (0.5% (vol/vol) Nonidet P-40, 150 mM NaCl, 20 mM Tris-HCl, pH 7.5, Complete Mini Protease Inhibitor Cocktail without EDTA (Roche) and 0.2 U/ml RNasin (Promega)). Anti-Flag antibody (F3165; Sigma) bound to protein G magnetic beads (Invitrogen) was incubated for 3 h at 4ºC with lysates and beads were washed three times with RNA IP lysis buffer. RNAs were eluted from the beads using Trizol reagent (Invitrogen) according to the manufacturer's instructions and analyzed by RT-qPCR. Proteins were eluted from the beads using SDS sample buffer (50 mM Tris-HCl, pH 6.8, 2% (wt/vol) SDS, 5% (vol/vol) β-mercaptoethanol, 10% (vol/vol) glycerol and bromophenol blue) and analyzed by Western blot with the indicated antibodies.

Morpholino delivery and ELISA for sera and culture supernatants

The antisense morpholino oligonucleotides used in this study were synthesized by Gene Tools, LLC and the following 25-mer morpholinos were used: Il6-SL-MO, 5′-CATTCATATTGTCAGTTCTTCGTAG-3′; and Ctrl-MO as the standard control oligo from Gene Tools, LLC (SC100), 5′-CCTCTTACCTCAGTTACAATTTATA-3′. For delivery of antisense morpholino oligonucleotides to HeLa cells or bone marrow

macrophages (BMMs) from wild-type mice, morpholinos were added to the medium at a final concentration of 2 μM in the presence of 6 μM Endo-Porter (Gene Tools, LLC) according to the manufacturer's protocol, and cells were incubated for 24 h and used in subsequent experiments. HeLa cells were used in luciferase assay as described above.

For measurement of Il6 and Tnf concentrations in culture supernatants from BMMs, BMMs were stimulated with LPS (100 ng/mL) and cytokine levels in culture supernatants were measured by cytokine-specific ELISA kits (R&D systems) following manufacturer's protocols. Cytokine mRNA levels in BMMs were analyzed by RT-qPCR as described above.

For measurement of Il6 and Tnf concentrations in sera from *Il6*$^{-/-}$ mice, BMMs (5 x 10^6 cells) were intraperitoneally (i.p.) transfused into *Il6*$^{-/-}$ mice (6-week-old, n = 4). The mice were injected with LPS (0.5 mg/kg of body weight, i.p.) 24 h after transfusion, and cytokine levels in sera were measured by cytokine-specific ELISA kits (R&D systems) following manufacturer's protocols.

HITS-CLIP

Flp-In 293 T-REx cell lines stably expressing FLAG/HA-tagged Reg1 protein were generated by co-transfection of pFRT/TO/FLAG/HA constructs with pOG44 (Invitrogen). Cells were selected by adding 15 μg/ml blasticidin and 100 μg/ml hygromycin (Invivogen). Expression of epitope-tagged proteins was induced by addition of 1 μg/ml doxycyclin. The expression of FLAG/HA tagged Reg1 protein was assessed by Western analysis using mouse anti-HA.11 monoclonal antibody (Covance). HITS-CLIP was performed essentially as described (Hafner et al., 2010). Briefly, UV-irradiated cells were lysed in NP-40 lysis buffer (50 mM HEPES-KOH at pH 7.4, 150 mM KCl, 2 mM EDTA, 0.5% (v/v) NP40, 0.5 mM DTT, complete EDTA-free protease inhibitor cocktail). After treatment with RNaseT1 (Fermentas) at final concentration of 0.5 unit/μl, immunoprecipitation was carried out with Flag magnetic

beads (SIGMA) from HEK293 cell extracts for 1 h at 4ºC. Following additional digestion by RNase T1 (Fermentas) at final concentration of 0.5 unit/µl, beads were incubated with calf intestinal phosphatase (NEB) and RNA fragments were radioactively end-labeled using T4 polynucleotide kinase (Fermentas). The crosslinked protein-RNA complexes were resolved on a 4-12% NuPAGE gel (Invitrogen). The SDS-PAGE gel was transferred to a nitrocellulose membrane (Whatman) and the protein-RNA complex migrating at an expected molecular weight was excised. RNA was isolated by Proteinase K (Roche) treatment and phenol-chloroform extraction, ligated to 3′ adapter and 5′ adapter, reverse transcribed and PCR-amplified. The amplified cDNA was sequenced on a HighSeq2000 (Illumina) with a 1x51 nt cycle.

Reg1 CLIP library processing

Reads from the Reg1 CLIP library were stripped of the adaptor sequence stepwise using Cutadapt, keeping the randomized nucleotides (Martin, 2011) (3′ Adapter, NN-TGGAATTCTCGGGTGCCAAGG; 5′ Adapter, GTTCAGAGTTCTACAGTCCGACGATC-NN). Reads that were less than 24 nucleotides in length or contained an ambiguous nucleotide were discarded. Reads were collapsed and then the randomized adapter nucleotides were trimmed using Flexbar (Dodt et al., 2012). The remaining reads were aligned to the human genome (hg19), with up to one mismatch allowed and ten alignment locations, with Bowtie version 0.12.7 (Langmead et al., 2009). Grouping of the reads was done using PARalyzer (Corcoran et al., 2011) to retain only those that mapped to a single genomic location for the minimum number of mismatches. Unique reads were grouped with a minimum of one nucleotide of overlap. Annotation of the resulting groups was performed as described (Ascano et al., 2012). The two libraries were intersected on group level with at least one nucleotide overlap. Full group level data are provided in Table S4.

Stem loop enrichment and stem loop sequence analyses

Group sequences were globally folded using RNAfold from the Vienna package (Lorenz et al., 2011) with default setting. Resulting stem loops have been quantified and compared against the number of retrieved stem loops after 1000 individual dinucleotide shuffles (using Dishuffle (Clote et al., 2005)) of the corresponding group sequences. Stem loop Postion weight matrixes were obtained using the web tool enoLOGOS (Workman et al., 2005), using stem loop sequences as input. RNA secondary structure and sequence motifs were predicted using Predict Motif (Rabani et al., 2008), using the entire Reg1 bound group sequence for the corresponding stem loop as input.

References for Extended Experimental Procedures

Anders, S., and Huber, W. (2010). Differential expression analysis for sequence count data. Genome Biol *11*, R106.

Ascano, M., Jr., Mukherjee, N., Bandaru, P., Miller, J.B., Nusbaum, J.D., Corcoran, D.L., Langlois, C., Munschauer, M., Dewell, S., Hafner, M., *et al.* (2012). FMRP targets distinct mRNA sequence elements to regulate protein expression. Nature *492*, 382-386.

Baltz, A.G., Munschauer, M., Schwanhausser, B., Vasile, A., Murakawa, Y., Schueler, M., Youngs, N., Penfold-Brown, D., Drew, K., Milek, M., *et al.* (2012). The mRNA-bound proteome and its global occupancy profile on protein-coding transcripts. Mol Cell *46*, 674-690.

Clote, P., Ferre, F., Kranakis, E., and Krizanc, D. (2005). Structural RNA has lower folding energy than random RNA of the same dinucleotide frequency. RNA *11*, 578-591.

Corcoran, D.L., Georgiev, S., Mukherjee, N., Gottwein, E., Skalsky, R.L., Keene, J.D., and Ohler, U. (2011). PARalyzer: definition of RNA binding sites from PAR-CLIP short-read sequence data. Genome Biol *12*, R79.

Dodt, M., Roehr, J.T., Ahmed, R., and Dieterich, C. (2012). FLEXBAR-Flexible Barcode and Adapter Processing for Next-Generation Sequencing Platforms. Biology (Basel) *1*, 895-905.

Hafner, M., Landthaler, M., Burger, L., Khorshid, M., Hausser, J., Berninger, P., Rothballer, A., Ascano, M., Jr., Jungkamp, A.C., Munschauer, M., *et al.* (2010). Transcriptome-wide identification of RNA-binding protein and microRNA target sites by PAR-CLIP. Cell *141*, 129-141.

Iwasaki, H., Takeuchi, O., Teraguchi, S., Matsushita, K., Uehata, T., Kuniyoshi, K., Satoh, T., Saitoh, T., Matsushita, M., Standley, D.M., *et al.* (2011). The IkappaB kinase complex regulates the stability of cytokine-encoding mRNA induced by TLR-IL-1R by controlling degradation of regnase-1. Nat Immunol *12*, 1167-1175.

Langmead, B., Trapnell, C., Pop, M., and Salzberg, S.L. (2009). Ultrafast and memory-efficient alignment of short DNA sequences to the human genome. Genome Biol *10*, R25.

Leppek, K., Schott, J., Reitter, S., Poetz, F., Hammond, M.C., and Stoecklin, G. (2013). Roquin promotes constitutive mRNA decay via a conserved class of stem-loop recognition motifs. Cell *153*, 869-881.

Lorenz, R., Bernhart, S.H., Honer Zu Siederdissen, C., Tafer, H., Flamm, C., Stadler, P.F., and Hofacker, I.L. (2011). ViennaRNA Package 2.0. Algorithms Mol Biol *6*, 26.

Martin, M. (2011). Cutadapt removes adapter sequences from high-throughput sequencing reads. EMBnet J *17*, 10-12.

Matsunaga, K., Saitoh, T., Tabata, K., Omori, H., Satoh, T., Kurotori, N., Maejima, I., Shirahama-Noda, K., Ichimura, T., Isobe, T., *et al.* (2009). Two Beclin 1-binding proteins, Atg14L and Rubicon, reciprocally regulate autophagy at different stages. Nat Cell Biol *11*, 385-396.

Matsushita, K., Takeuchi, O., Standley, D.M., Kumagai, Y., Kawagoe, T., Miyake, T., Satoh, T., Kato, H., Tsujimura, T., Nakamura, H., *et al.* (2009). Zc3h12a is an RNase essential for controlling immune responses by regulating mRNA decay. Nature *458*, 1185-1190.

Mishima, Y., Fukao, A., Kishimoto, T., Sakamoto, H., Fujiwara, T., and Inoue, K. (2012).

Translational inhibition by deadenylation-independent mechanisms is central to microRNA-mediated silencing in zebrafish. Proc Natl Acad Sci U S A *109*, 1104-1109.
Mudhasani, R., Zhu, Z., Hutvagner, G., Eischen, C.M., Lyle, S., Hall, L.L., Lawrence, J.B., Imbalzano, A.N., and Jones, S.N. (2008). Loss of miRNA biogenesis induces p19Arf-p53 signaling and senescence in primary cells. J Cell Biol *181*, 1055-1063.
Rabani, M., Kertesz, M., and Segal, E. (2008). Computational prediction of RNA structural motifs involved in posttranscriptional regulatory processes. Proc Natl Acad Sci U S A *105*, 14885-14890.
Subramanian, A., Tamayo, P., Mootha, V.K., Mukherjee, S., Ebert, B.L., Gillette, M.A., Paulovich, A., Pomeroy, S.L., Golub, T.R., Lander, E.S., *et al.* (2005). Gene set enrichment analysis: a knowledge-based approach for interpreting genome-wide expression profiles. Proc Natl Acad Sci U S A *102*, 15545-15550.
Wilkinson, K.A., Merino, E.J., and Weeks, K.M. (2006). Selective 2'-hydroxyl acylation analyzed by primer extension (SHAPE): quantitative RNA structure analysis at single nucleotide resolution. Nat Protoc *1*, 1610-1616.
Workman, C.T., Yin, Y., Corcoran, D.L., Ideker, T., Stormo, G.D., and Benos, P.V. (2005). enoLOGOS: a versatile web tool for energy normalized sequence logos. Nucleic Acids Res *33*, W389-392.
Zinzalla, V., Stracka, D., Oppliger, W., and Hall, M.N. (2011). Activation of mTORC2 by association with the ribosome. Cell *144*, 757-768.

Supplemental Figure Legends

Figure S1. Identification of novel Reg1 target molecules, related to Figure 1

(A) Reg1 endonucleolytically cleaved the Il6 3′UTR (1-403) *in vitro* cleavage assay. Indicated circular or linear Il6 3′UTR RNAs were incubated with increasing amounts of recombinant Reg1 proteins.

(B) Coomassie Brilliant Blue-stained SDS gel showing purified recombinant WT or D141N mutant Reg1 proteins.

(C) Reg1 cleaved the (84-103) SL of Il6-3′UTR in vitro cleavage assay. Indicated Il6 RNAs were incubated with increasing amounts of recombinant Reg1 proteins.

(D) Luciferase activity of HeLa cells transfected with reporter plasmids expressing 5XBoxB and Il6 3′UTR, together with indicated expression plasmids. The gene encoding Renilla luciferase was transfected simultaneously as an internal control. Data are mean ± SD.

(E) MEFs from *Reg1*$^{-/-}$ and WT mice were stimulated with LPS (100 ng/mL) and miRNA expression levels were analyzed by RT-qPCR. Data are mean ± SD (n = 3).

(F) Structural models of WT and D141N mutant Reg1 PIN domains. Cartoon representations of homology models of the PIN domain (residues 132-295) of WT and D141N mouse Reg1 after 10 ns of explicit water MD. Regions colored red are predicted to interact with RNA.

(G) Luciferase activity of HeLa cells transfected with indicated reporter and indicated Roquin expression plasmids. Roquin-NT is an N-terminal fragment (amino acids [aa] 2–441), which is responsible for RNA-binding. Data are mean ± SD.

Figure S2. Identification of Reg1-recognition motives, related to Figure 1

(A, D, E, I) Luciferase activity of HeLa cells transfected with indicated reporter and expression plasmids. Data are mean ± SD.

(B, H) Schematic representation of Reg1-recognition sequences in mouse *Nfkbiz* (B)

and *Ptgs2* (H) together with an alignment of 5 mammalian sequences.

(C, F, J,) Schematic representation of Reg1-recognition stem-loop structures in *Nfkbiz* (C), *Ptgs2* (F), TNE-CDE (J).

(G) SHAPE analysis of in *vitro* synthesized mPtgs2 3′UTR (1204-1237) RNA.

Figure S3. Reg1 recognizes stem-loop motifs in 3′UTRs, related to Figure 2

(A, B) Schematic representation of TNF-CDE (A) and an artificial stem-loop (B) structures.

(C) SHAPE analysis of in vitro synthesized a "UAU-loop" stem-loop RNA.

(D, E) Luciferase activity of HeLa cells transfected with indicated reporter and Reg1 expression plasmids. Data are mean ± SD.

(F–H) mRNAs associated with Reg1 in HeLa cells transfected with indicated expression plasmids were recovered by RNA IP and analyzed RT-qPCR. Data are mean ± SD. Lower panels show immunoblots probed with an anti-Flag antibody.

Figure S4. Reg1 and Roquin degrade mRNAs via distinct mechanisms, related to Figure 3

(A) Top: Degradation of Il6CDS-3′UTR mRNA under co-transfection with Caf1a-AA or Dcp2-AA was measured as in Figure 4B. Bottom: Quantification of the autoradiographs. Data are mean ± SD.

(B and C) Immunofluorescent microscopy showing the localization of Roquin to PB and SG. NIH3T3 (B) and HeLa (C) cells transiently-expressing EGFP-tagged Roquin were treated with arsenite for 1 h and analyzed by confocal fluorescence microscopy.

(D) Immunoblot analysis of endogenous and Flag-Reg1 expression in Flag-Reg1 stably expressing NIH3T3 cells. The levels of Reg1 detected by ant-Reg1 Ab was quantified and shown.

(E) Immunofluorescent microscopy showing the localization of Reg1 to the cytoplasm

and ER, but not to PB and SG. HeLa cells transiently-expressing Flag-Reg1 were analyzed by confocal fluorescence microscopy.

(F) Fluorescence *in situ* hybridization of *Ptgs2* and fluorescence immunostaining of Dcp1a (PB marker) in HeLa cells transfected with siRNA specific for Reg1 or Roquin-1/2 and stimulated with IL-1β for 4 h.

(G) Quantification of *Ptgs2* mRNAs in Figure S4F. Data are mean ± SD.

(H) Quantification of *Ptgs2* mRNAs localized in PB (%) in Figure S4F. Data are mean ± SD.

Figure S5. Treatments with protein synthesis inhibitors have no effect on the localization of Reg1, related to Figure 4

(A) NIH3T3 cells expressing Flag-Reg1 were treated with anisomycin or CHX for 2 h and analyzed by confocal fluorescence microscopy.

(B) Immunoblot analysis of Reg1 transiently-expressed in Tet-off 293 cells under treatment with anisomycin or CHX as in Figure 4B and 4C.

(C) IRES-dependent translation initiation had no effect on Reg1-mediated RNA decay. Degradation of IRES-*Il6* mRNA was inserted in upstream of *Il6* CDS, was measured as in Figure 4B.

(D) Quantification of the autoradiographs in Figure S5C. Data are mean ± SD.

Figure S6. Essential roles of UPF1 in Reg1-mediated mRNA decay, related to Figure 6.

(A) Immunoblot analysis of UPF1 and Reg1 in RAW264.7 macrophages transfected with indicated siRNAs.

(B) Luciferase activity of RAW264.7 macrophages transfected with indicated siRNA, reporter and Reg1 expression plasmids. Data are mean ± SD.

(C) Luciferase activity of RAW264.7 macrophages transfected with indicated siRNA,

reporter and Roquin expression plasmids. Data are mean ± SD.

(D) RAW264.7 macrophages were transfected with the indicated siRNAs and stimulated with LPS. RNA expression profiles were analyzed by RT-qPCR. Data are mean ± SD.

(E) Immunoblot analysis of Reg1 in HeLa cells transfected with indicated expression plasmids.

(F) mRNAs associated with Reg1 in Tet-off 293 cells treated with anisomycin were recovered by RNA IP and analyzed RT-qPCR. Data are mean ± SD.

(G) Immunoblot analysis of UPF1 and its helicase dead mutant (DEAA) co-immunoprecipitated with Flag-Reg1-WT transiently-expressed in HeLa cells.

Figure S7. Inflammatory gene expression in cells defective in the Reg1 and Roquin to TNF stimulation, related to Figure 7

(A) HeLe cells transiently-expressing Flag-Reg1-D141N were analyzed by confocal fluorescence microscopy.

(B) Luciferase activity of HeLa cells transfected with indicated reporter and Reg1 and Roquin expression plasmids. Data are mean ± SD.

(C) The ratio of non-polysome and polysome RNA to total RNA in Figure 3H.

(D) MEFs from *Reg1*$^{-/-}$; *Roquin*$^{san/san}$, *Reg1*$^{-/-}$, *Roquin*$^{san/san}$ or WT mice were stimulated with TNF (10 ng/mL) and RNA expression profiles were analyzed by RT-qPCR. Data are mean ± SD.

(E) Heat map of the expression of selected LPS-inducible genes on the basis of transcriptome analysis of WT, *Reg1*$^{-/-}$; *Roquin*$^{San/San}$, *Reg1*$^{-/-}$ and *Roquin*$^{San/San}$ MEFs.

(F) GSEA of overlap between Reg1 (left) or Roquin (right) target genes (RIP-seq based) and Roquin$^{San/San}$ enrichment (transcriptome analysis based). An ES plot is shown with genes ranked according to their Roquin$^{San/San}$ enrichment p value. In lower panels, the ranks of Reg1 (left) or Roquin (right) target genes are indicated (blue lines).

Legends for Supplementary Tables.

Table S1. RNA sequencing data from Reg1 IP experiments, related to Figure 1

Table S2. Gene ontology (GO) annotations enriched for the 68 Reg1-interacting mRNAs, Related to Figure 1

Table S3. RNA sequencing data from Roquin-1 IP experiments, Related to Figure 2

Table S4. RNA sequencing data from Reg1 HITS-CLIP experiments, Related to Figure 2

Table S5. Ribosome is a candidate complex as Reg1-associated complex, Related to Figure 5

Proteins enriched by iTRAQ-based proteomic identifying as Reg1-associated proteins. Control or Flag-Reg1 immunoprecipitates from RAW cells was labeled with iTRAQ reagent 114 or 117, respectively. The contents of each iTRAQ reagent-labeled sample were combined and analyzed by LC-MS/MS. Based on a 80% confidence level (< 20% 117/114 variability), cutoff values of 1.2-fold for up-regulated proteins were used to define candidate proteins as Reg1-associated proteins.

Table S6. Transcriptome analysis from *Reg1*$^{-/-}$; *Roquin*$^{San/San}$ double mutant MEFs, Related to Figure 7

Table S7. Primers used for quantitative PCR analysis and the preparation of Northern blot probes, Related to Experimental Procedures

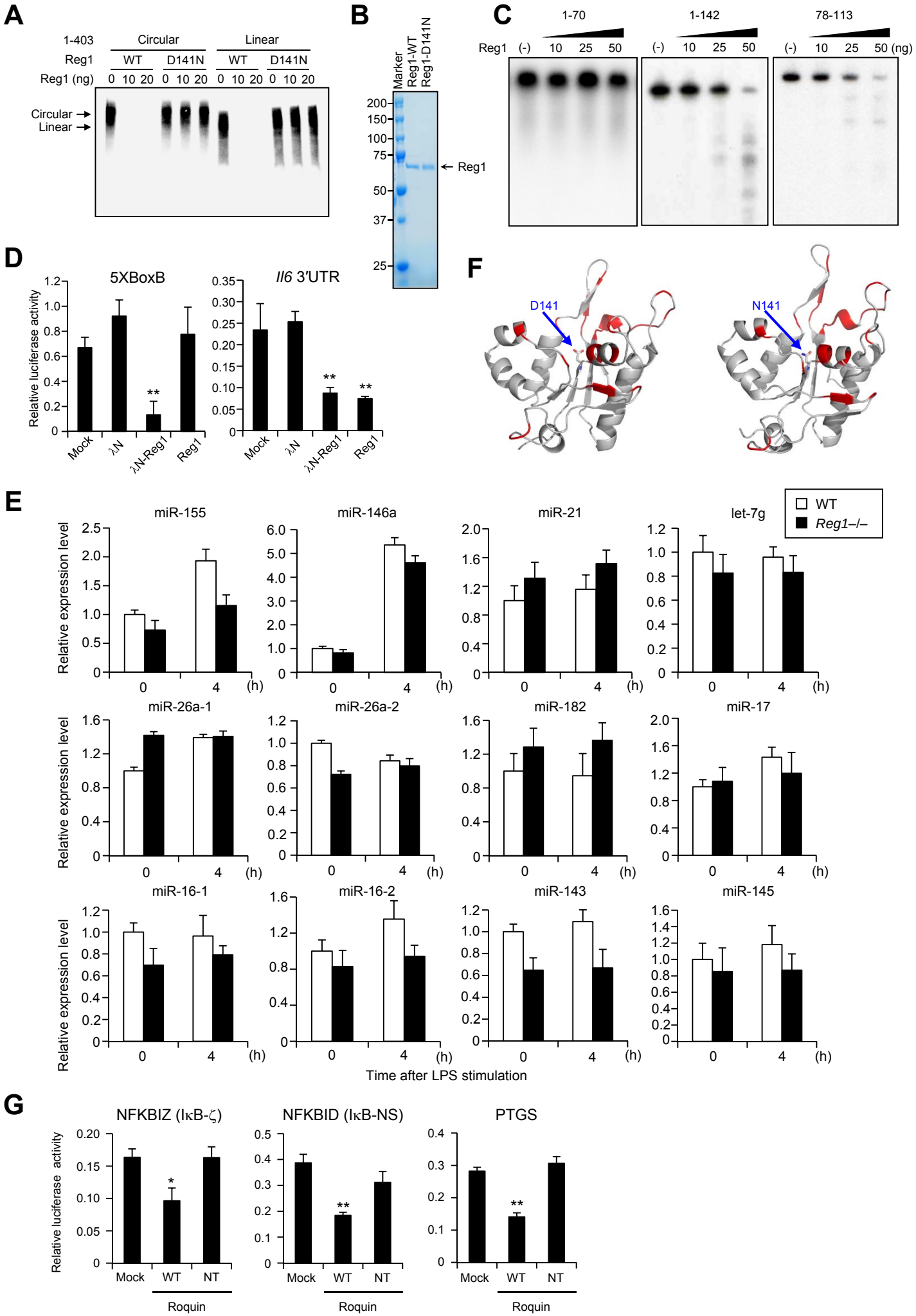
A
1-403
Circular
Linear
Reg1
WT
D141N
WT
D141N
Reg1 (ng)
0 10 20 0 10 20 0 10 20 0 10 20
Circular
Linear
B
Marker
Reg1-WT
Reg1-D141N
200
150
100
75
50
37
25
Reg1
C
1-70
1-142
78-113
Reg1 (-) 10 25 50 (-) 10 25 50 (-) 10 25 50 (ng)
D
5XBoxB
Il6 3′UTR
Relative luciferase activity
Mock
λN
λN-Reg1
Reg1
F
D141
N141
E
WT
Reg1–/–
miR-155
miR-146a
miR-21
let-7g
miR-26a-1
miR-26a-2
miR-182
miR-17
miR-16-1
miR-16-2
miR-143
miR-145
Relative expression level
(h)
Time after LPS stimulation
G
NFKBIZ (IκB-ζ)
NFKBID (IκB-NS)
PTGS
Relative luciferase activity
Mock
WT
NT
Roquin

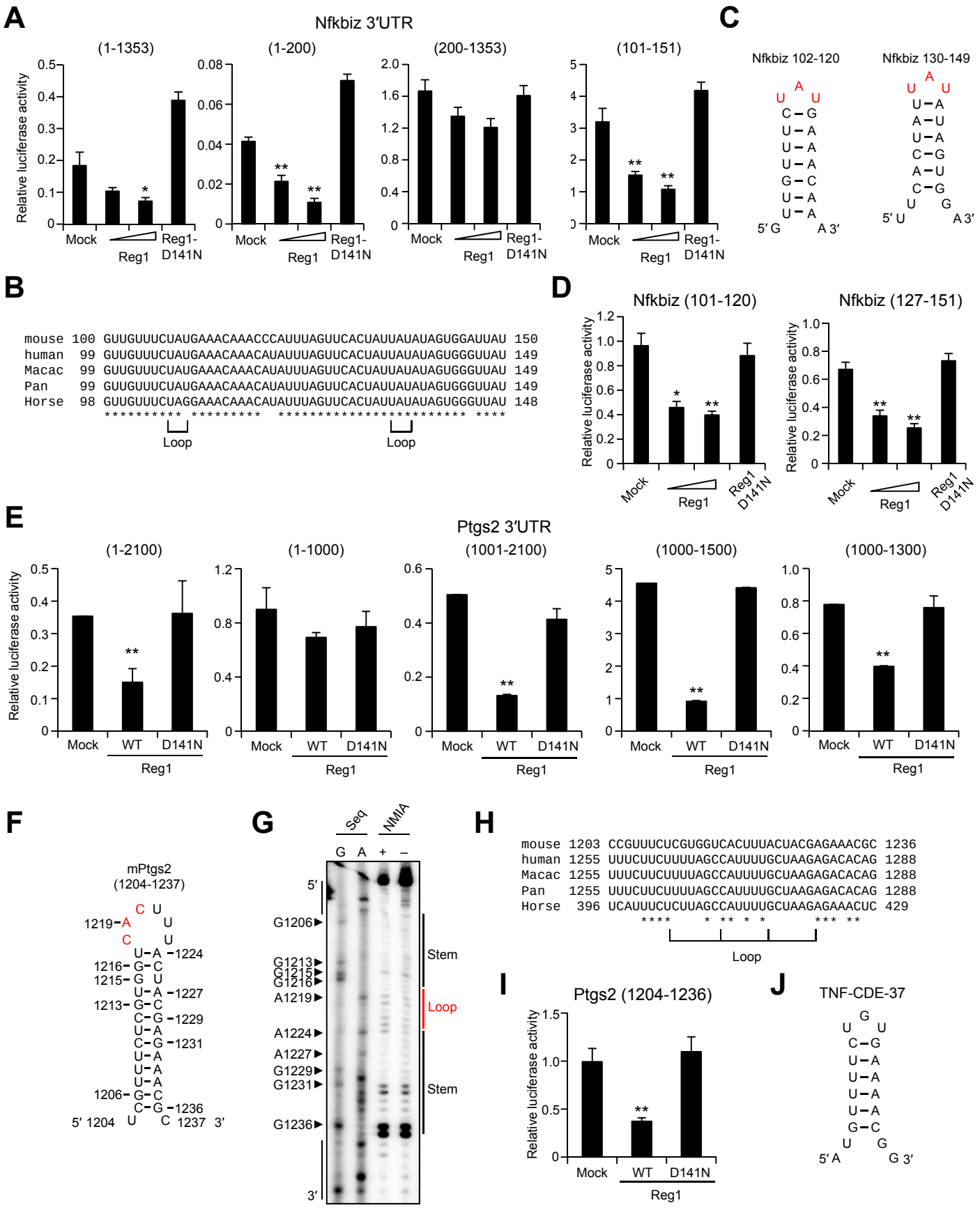
A
Nfkbiz 3′UTR
(1-1353)
(1-200)
(200-1353)
(101-151)
Relative luciferase activity
Mock
Reg1
Reg1-D141N
B
mouse 100 GUUGUUUCUAUGAAACAAACCCAUUUAGUUCACUAUUAUAUAGUGGAUUAU 150
human 99 GUUGUUUCUAUGAAACAAACAUAUUUAGUUCACUAUUAUAUAGUGGGUUAU 149
Macac 99 GUUGUUUCUAUGAAACAAACAUAUUUAGUUCACUAUUAUAUAGUGGGUUAU 149
Pan 99 GUUGUUUCUAUGAAACAAACAUAUUUAGUUCACUAUUAUAUAGUGGGUUAU 149
Horse 98 GUUGUUUCUAGGAAACAAACAUAUUUAGUUCACUAUUAUAUAGUGGGUUAU 148
Loop
Loop
C
Nfkbiz 102-120
Nfkbiz 130-149
5′ G
A 3′
5′ U
A 3′
D
Nfkbiz (101-120)
Nfkbiz (127-151)
Relative luciferase activity
Mock
Reg1
Reg1 D141N
E
Ptgs2 3′UTR
(1-2100)
(1-1000)
(1001-2100)
(1000-1500)
(1000-1300)
Relative luciferase activity
Mock
WT
D141N
Reg1
F
mPtgs2
(1204-1237)
5′ 1204
C 1237 3′
G
Seq
NMIA
G A + –
5′
3′
G1206
G1213
G1215
G1216
A1219
A1224
A1227
G1229
G1231
G1236
Stem
Loop
Stem
H
mouse 1203 CCGUUUCUCGUGGUCACUUUACUACGAGAAACGC 1236
human 1255 UUUCUUCUUUUAGCCAUUUUGCUAAGAGACACAG 1288
Macac 1255 UUUCUUCUUUUAGCCAUUUUGCUAAGAGACACAG 1288
Pan 1255 UUUCUUCUUUUAGCCAUUUUGCUAAGAGACACAG 1288
Horse 396 UCAUUUCUCUUAGCCAUUUUGCUAAGAGAAACUC 429
Loop
I
Ptgs2 (1204-1236)
Relative luciferase activity
Mock
WT
D141N
Reg1
J
TNF-CDE-37
5′ A
G 3′

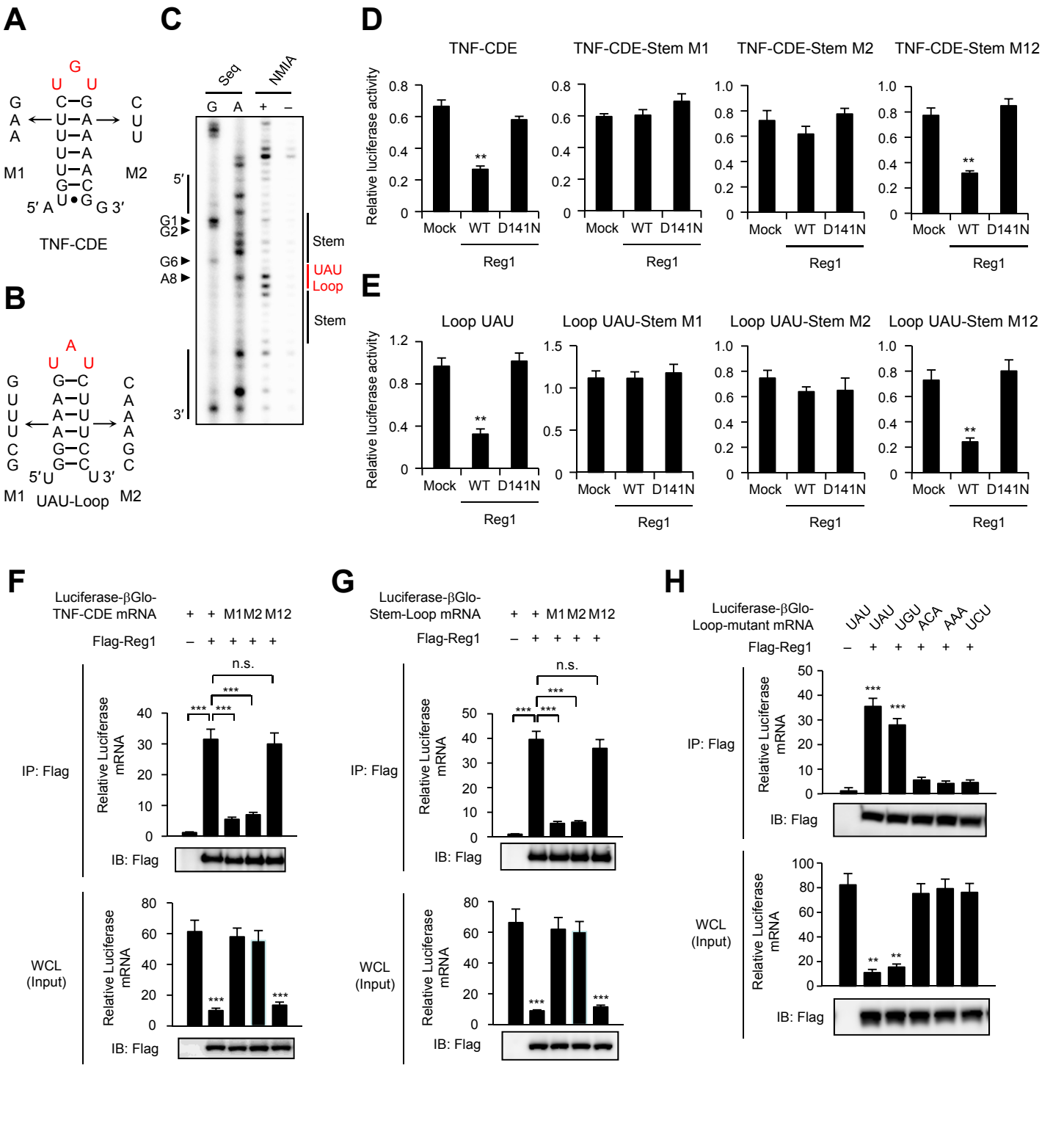
A
B
C
D
E
F
G
H
TNF-CDE
UAU-Loop
M1
M2
5′
3′
Seq
NMIA
Stem
UAU Loop
G1
G2
G6
A8
TNF-CDE
TNF-CDE-Stem M1
TNF-CDE-Stem M2
TNF-CDE-Stem M12
Loop UAU
Loop UAU-Stem M1
Loop UAU-Stem M2
Loop UAU-Stem M12
Relative luciferase activity
Mock
WT
D141N
Reg1
Luciferase-βGlo-TNF-CDE mRNA
Luciferase-βGlo-Stem-Loop mRNA
Luciferase-βGlo-Loop-mutant mRNA
Flag-Reg1
M1 M2 M12
UAU UAU UGU ACA AAA UCU
IP: Flag
WCL (Input)
Relative Luciferase mRNA
IB: Flag
n.s.

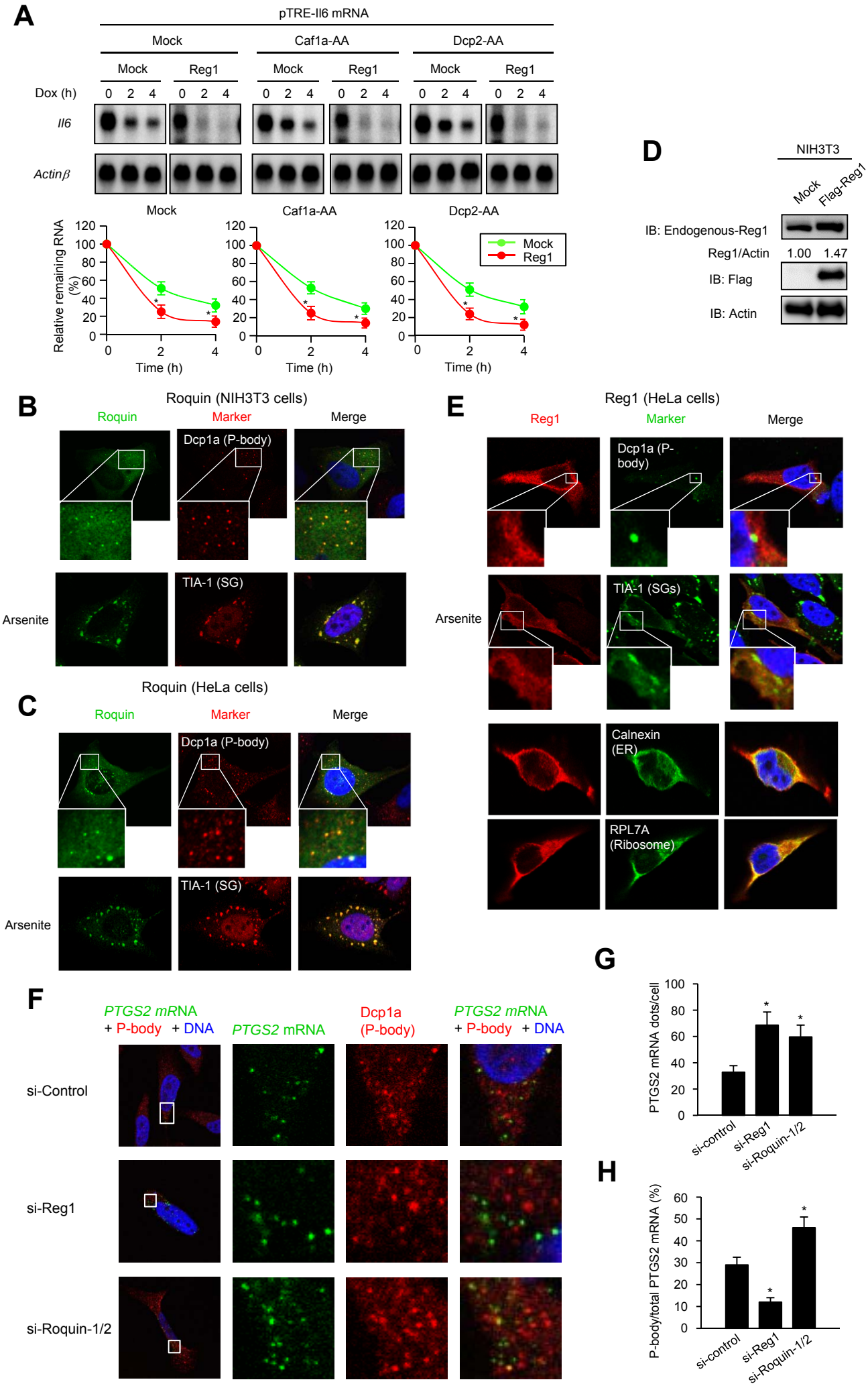
A
pTRE-Il6 mRNA
Mock
Caf1a-AA
Dcp2-AA
Mock
Reg1
Dox (h)
0 2 4
Il6
Actinβ
Relative remaining RNA (%)
Time (h)
Mock
Reg1
D
NIH3T3
Mock
Flag-Reg1
IB: Endogenous-Reg1
Reg1/Actin
1.00 1.47
IB: Flag
IB: Actin
B
Roquin (NIH3T3 cells)
Roquin
Marker
Merge
Dcp1a (P-body)
TIA-1 (SG)
Arsenite
C
Roquin (HeLa cells)
E
Reg1 (HeLa cells)
Reg1
Dcp1a (P-body)
TIA-1 (SGs)
Calnexin (ER)
RPL7A (Ribosome)
F
PTGS2 mRNA + P-body + DNA
PTGS2 mRNA
Dcp1a (P-body)
si-Control
si-Reg1
si-Roquin-1/2
G
PTGS2 mRNA dots/cell
si-control
si-Reg1
si-Roquin-1/2
H
P-body/total PTGS2 mRNA (%)

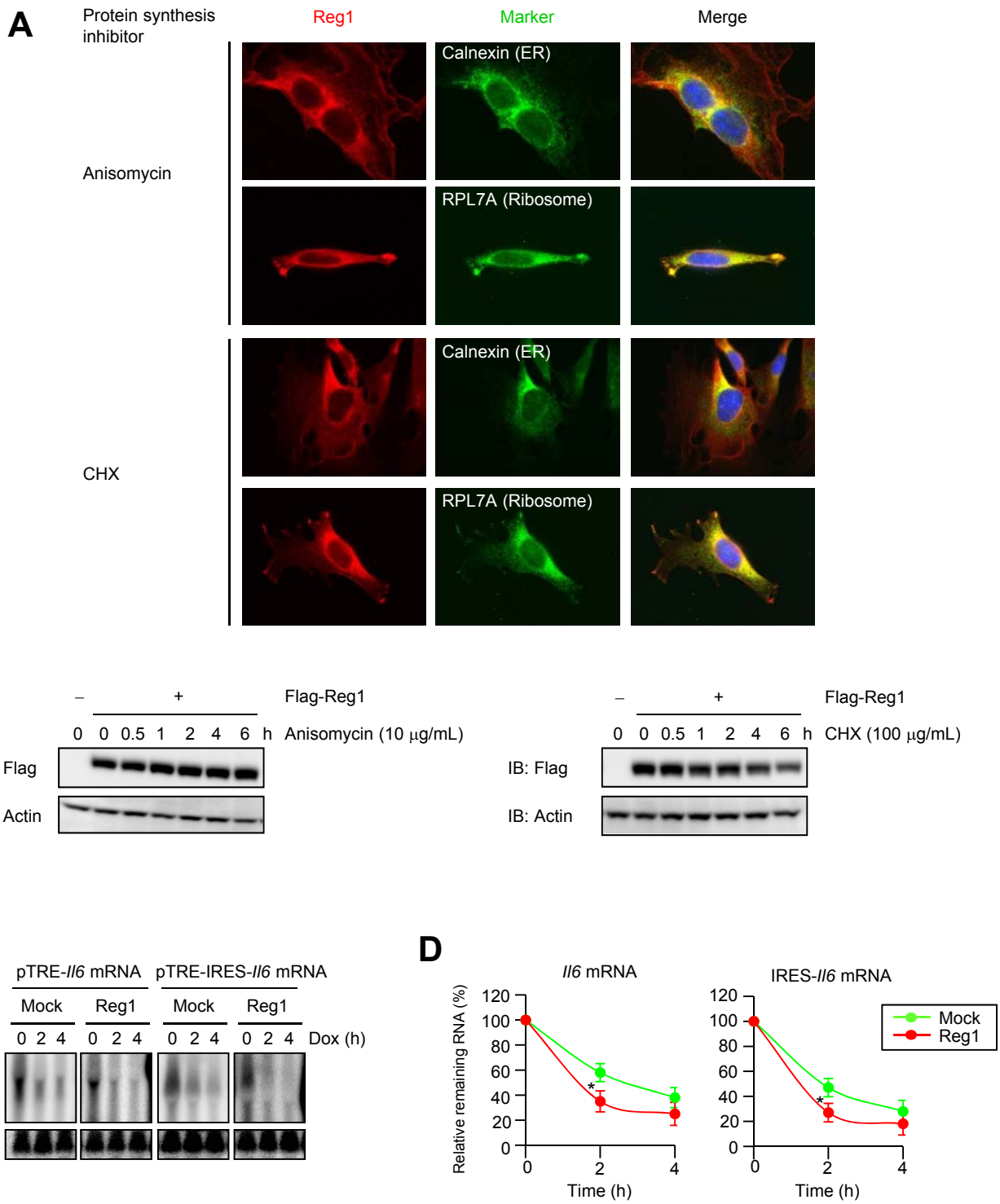
A
Protein synthesis inhibitor
Reg1
Marker
Merge
Anisomycin
Calnexin (ER)
RPL7A (Ribosome)
CHX
Calnexin (ER)
RPL7A (Ribosome)
B
–
+
Flag-Reg1
0 0 0.5 1 2 4 6 h
Anisomycin (10 μg/mL)
IB: Flag
IB: Actin
–
+
Flag-Reg1
0 0 0.5 1 2 4 6 h
CHX (100 μg/mL)
IB: Flag
IB: Actin
C
pTRE-Il6 mRNA
pTRE-IRES-Il6 mRNA
Mock
Reg1
Mock
Reg1
0 2 4 0 2 4 0 2 4 0 2 4
Dox (h)
Il6
Actinβ
D
Il6 mRNA
IRES-Il6 mRNA
Relative remaining RNA (%)
120
100
80
60
40
20
0
0
2
4
Time (h)
Mock
Reg1
*
*

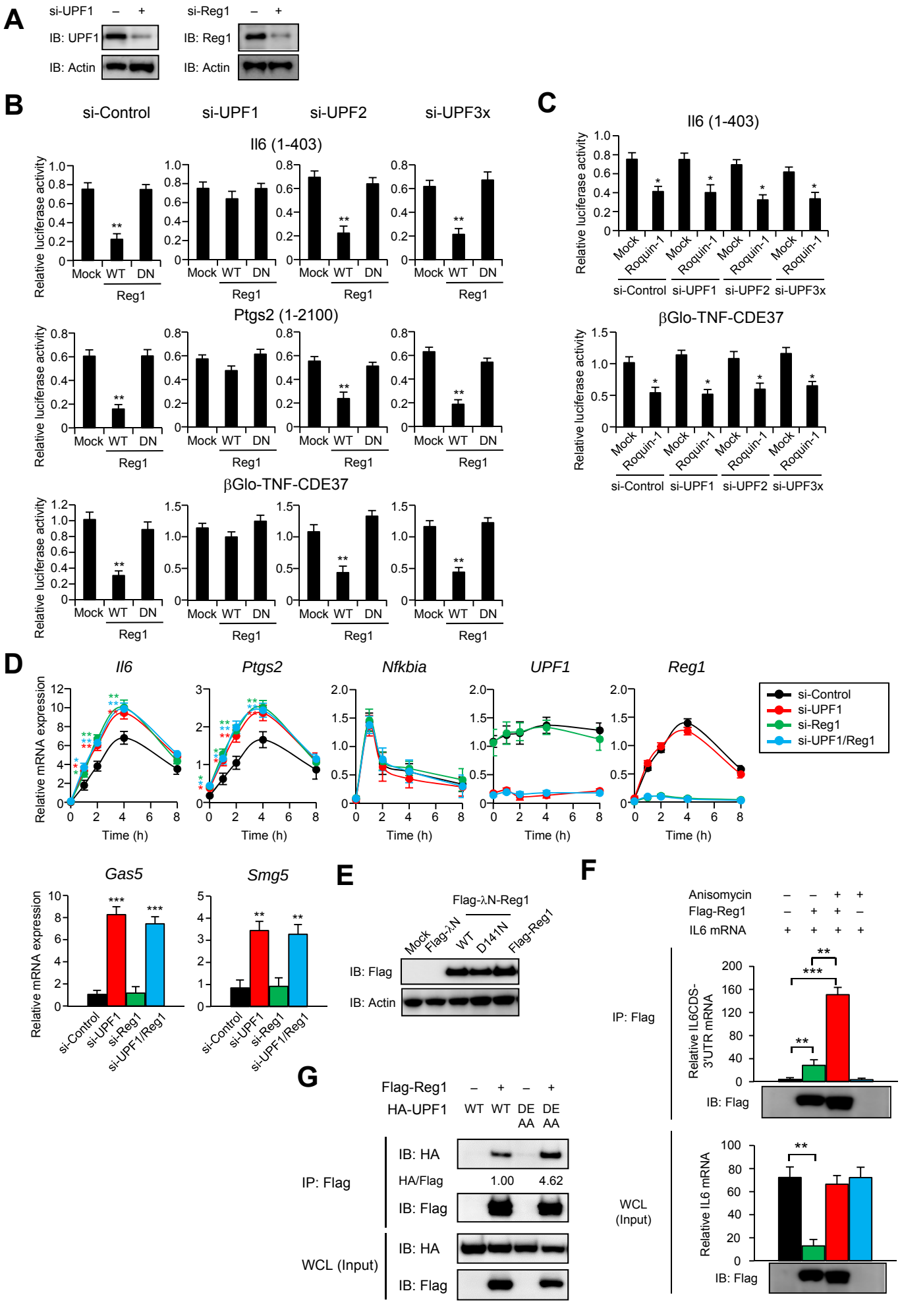
A
si-UPF1 – +
IB: UPF1
IB: Actin
si-Reg1 – +
IB: Reg1
IB: Actin
B
si-Control
si-UPF1
si-UPF2
si-UPF3x
Il6 (1-403)
Ptgs2 (1-2100)
βGlo-TNF-CDE37
Relative luciferase activity
Mock WT DN
Reg1
C
Il6 (1-403)
βGlo-TNF-CDE37
Relative luciferase activity
Mock Roquin-1
si-Control si-UPF1 si-UPF2 si-UPF3x
D
Il6
Ptgs2
Nfkbia
UPF1
Reg1
Relative mRNA expression
Time (h)
si-Control
si-UPF1
si-Reg1
si-UPF1/Reg1
Gas5
Smg5
E
Flag-λN-Reg1
Mock
Flag-λN
WT
D141N
Flag-Reg1
IB: Flag
IB: Actin
F
Anisomycin – – + +
Flag-Reg1 – + + –
IL6 mRNA + + + +
IP: Flag
Relative IL6CDS-3'UTR mRNA
IB: Flag
WCL (Input)
Relative IL6 mRNA
G
Flag-Reg1 – + – +
HA-UPF1 WT WT DE AA DE AA
IP: Flag
IB: HA
HA/Flag 1.00 4.62
IB: Flag
WCL (Input)
IB: HA
IB: Flag

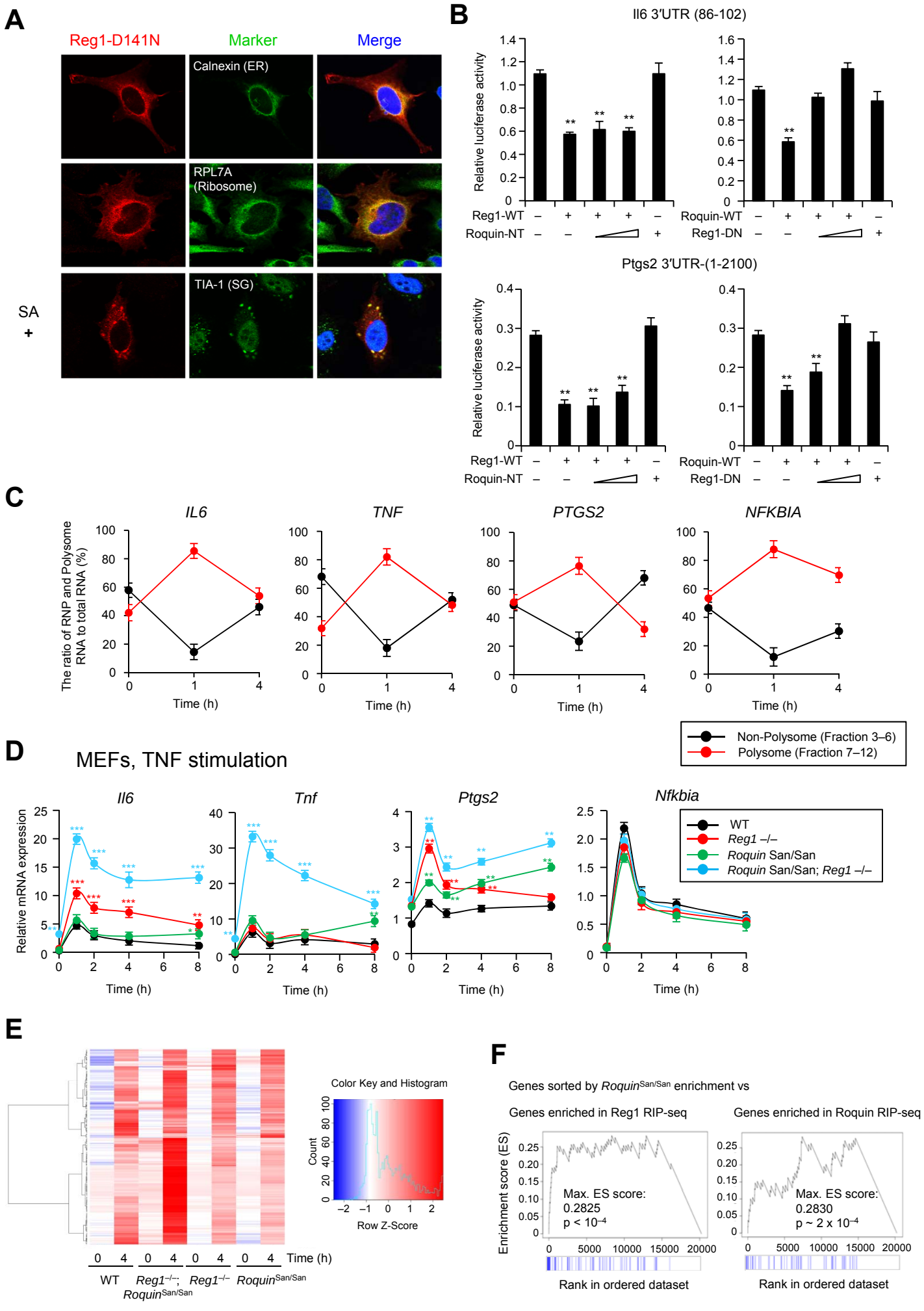
A
Reg1-D141N
Marker
Merge
Calnexin (ER)
RPL7A (Ribosome)
TIA-1 (SG)
SA +
B
Il6 3′UTR (86-102)
Relative luciferase activity
Reg1-WT
Roquin-NT
Roquin-WT
Reg1-DN
Ptgs2 3′UTR-(1-2100)
C
IL6
TNF
PTGS2
NFKBIA
The ratio of RNP and Polysome RNA to total RNA (%)
Time (h)
Non-Polysome (Fraction 3–6)
Polysome (Fraction 7–12)
D
MEFs, TNF stimulation
Il6
Tnf
Ptgs2
Nfkbia
Relative mRNA expression
WT
Reg1 –/–
Roquin San/San
Roquin San/San; Reg1 –/–
E
Color Key and Histogram
Count
Row Z-Score
Time (h)
WT
Reg1−/−; Roquin San/San
Reg1−/−
Roquin San/San
F
Genes sorted by Roquin San/San enrichment vs
Genes enriched in Reg1 RIP-seq
Genes enriched in Roquin RIP-seq
Enrichment score (ES)
Max. ES score: 0.2825
p < 10−4
Max. ES score: 0.2830
p ~ 2 x 10−4
Rank in ordered dataset

Table S2. Functional Categories of Reg1 target genes discovered by RIP-Sequencing analysis.

Rank	Gene ontology term (biological process)	Pvalue	OddsRatio	ExpCount	Count	Size	ID
1	response to wounding	1.32E-08	6.333951	4.25545675	19	1128	GO:0009611
2	inflammatory response	4.47E-08	8.585926	1.94664511	13	516	GO:0006954
3	response to molecule of bacterial origin	1.36E-07	13.040962	0.84128267	9	223	GO:0002237
4	positive regulation of smooth muscle cell proliferation	3.32E-07	42.543253	0.14713015	5	39	GO:0048661
5	regulation of nitric oxide biosynthetic process	4.87E-07	39.085851	0.15844786	5	42	GO:0045428
6	response to bacterium	9.06E-07	8.863915	1.37321477	10	364	GO:0009617
7	cardiovascular system development	1.15E-06	5.906329	3.0331447	14	804	GO:0072358
8	circulatory system development	1.15E-06	5.906329	3.0331447	14	804	GO:0072359
9	response to lipopolysaccharide	1.20E-06	11.915033	0.79978442	8	212	GO:0032496
10	nitric oxide biosynthetic process	1.45E-06	30.748853	0.19617354	5	52	GO:0006809

Table S5. Ribosome and UPF1 is a candidate complex as Reg1-associated complex, related to Figure 5
Proteins enriched by iTRAQ-based proteomic identifying as Reg1-associated proteins. Control or Flag-Reg1 immunoprecipitates from RAW cells was labeled with iTRAQ reagent 114 or 117, respectively. The contents of each iTRAQ reagent-labeled sample were combined and analyzed by LC-MS/MS. Based on a 80% confidence level (< 20% 117/114 variability), cutoff values of 1.2-fold for up-regulated proteins were used to define candidate proteins as Reg1-associated proteins.

RAW cells

Accession No.	Protein Name	Fold Change (117/114)	117/114 Variability [%]
Q5D1E7	Zinc finger CCCH domain-containing protein 12A (Zc3h12a)	4.618	3.8
P17156	Heat shock-related 70 kDa protein 2 (Hspa2)	1.433	0.7
Q9D8E6	60S ribosomal protein L4 (Rpl4)	1.371	4.3
P62267	40S ribosomal protein S23 (Rps23)	1.369	13.6
P62274	40S ribosomal protein S29 (Rps29)	1.322	7.4
P05213	Tubulin alpha-1B chain (Tuba1b)	1.320	0.6
Q9EPU0	UPF1 regulator of nonsense transcripts homolog (Upf1)	1.292	15.2
Q8VC57	BTB/POZ domain-containing protein KCTD5 (Kctd5)	1.288	0.8
P61255	60S ribosomal protein L26 (Rpl26)	1.288	6.4
Q9JMH9	Myosin-XVIIIa (Myo18a)	1.278	5.0
Q03265	ATP synthase subunit alpha, mitochondrial (Atp5a1)	1.275	8.6
P62702	40S ribosomal protein S4, X isoform (Rps4x)	1.262	6.6
P62908	40S ribosomal protein S3 (Rps3)	1.249	2.3
P14131	40S ribosomal protein S16 (Rps16)	1.227	4.3
P67984	60S ribosomal protein L22 (Rpl22)	1.221	11.7
P35980	60S ribosomal protein L18 (Rpl18)	1.214	1.4
Q8BGD9	Eukaryotic translation initiation factor 4B (Eif4b)	1.209	14.2
P56959	RNA-binding protein FUS (Fus)	1.207	1.1
P25444	40S ribosomal protein S2 (Rps2)	1.202	10.3
P20029	78 kDa glucose-regulated protein (Hspa5)	1.201	1.0
Q9JHJ0	Tropomodulin-3 (Tmod3)	1.200	6.6
P62900	60S ribosomal protein L31 (Rpl31)	1.200	5.3

List of primers

Table S7. Primers used for quantitative PCR analysis

Gene	Sequence (5′ to 3′)
Mouse Il6 (Forward)	GTAGCTATGGTACTCCAGAAGAC
Mouse Il6 (Reverse)	ACGATGATGCACTTGCAGAA
Mouse Tnf (Forward)	CCCTCACACTCAGATCATCTTCT
Mouse Tnf (Reverse)	GCTACGACGTGGGCTACAG
Mouse Zc3h12a (Forward)	CGAGAGGCAGGAGTGGAAAC
Mouse Zc3h12a (Reverse)	CTTACGAAGGAAGTTGTCCAGGCTAG
Mouse Roquin (Rc3h1) (Forward)	GACCAGACCACTATCAATACGGAC
Mouse Roquin (Rc3h1) (Reverse)	CACTGCTGAGTGGCTTCAGGTAC
Mouse Roquin2 (Rc3h2) (Forward)	CACTAGGAGAAAGAACTGTGAC
Mouse Roquin2 (Rc3h2) (Reverse)	GCAGAACCATCTTCTAATGCCAGC
Mouse Nfkbiz (IkBz) (Forward)	CTCCGACTCCTCCGATTTCTC
Mouse Nfkbiz (IkBz) (Reverse)	GCTTGTTGCTTCGGATGTGTAG
Mouse Nfkbid (IkBNS) (Forward)	GAGCTCACATATTGGCTCTG
Mouse Nfkbid (IkBNS) (Reverse)	GAATATCCAGCTGTCGGTAC
Mouse Ptgs2 (Forward)	CTTGCTGTTCCAATCCATGTC
Mouse Ptgs2 (Reverse)	GTTCCAGACTCCCTTGAAGTG
Mouse Icos (Forward)	GTGTCTTTGTCTTCTGCTTC
Mouse Icos (Reverse)	GAGGACTTCTCTCTCTCTGAAC
Mouse UPF1 (Forward)	GCTGAACTTCGAGGAAGATG
Mouse UPF1 (Reverse)	CTTCCTTGCATTTTGCCCTC
Mouse UPF2 (Forward)	CATTAGTCCGGAGAAGCAGC
Mouse UPF2 (Reverse)	GTGCCTGTCCTCACTTAGCTC
Mouse UPF3x (Forward)	GGACCGATTTGATGGCTATG
Mouse UPF3x (Reverse)	CATTGTCTGTGGCATAACTCTC
Mouse Cxcl-1 (Forward)	CCATGGCTGGGATTCACCTC
Mouse Cxcl-1 (Reverse)	CTCCGTTACTTGGGGACACC
Mouse Cxcl-2 (Forward)	CTGTCAATGCCTGAAGACCCTG
Mouse Cxcl-2 (Reverse)	CTCCTTTCCAGGTCAGTTAGC
Mouse Cxcl-3 (Forward)	CTGTTGTGGCCAGTGAGCTG
Mouse Cxcl-3 (Reverse)	GATGATTATCTGAAGCCTGG
Mouse Nfkbia (IkBa) (Forward)	GAGGAGTACGAGCAAATGGTG
Mouse Nfkbia (IkBa) (Reverse)	CCTGACCAATGACTTCCATG
Mouse Gas5 (Forward)	CAGGTATTAATGGGTCACCTC
Mouse Gas5 (Reverse)	CTTCTATTTGAGCCTCCATCC
Mouse Smg5 (Forward)	CAGAGAACGTTAGCCTGAGG
Mouse Smg5 (Reverse)	CTGTAGGCACATTCCAAGGTG
Mouse Mafk (Forward)	CTAATCCCAAGCCCAACAAG
Mouse Mafk (Reverse)	GTAGCCTCTGTTCTTGAGTGTG
Mouse Stau1 (Forward)	GCTGTTCTGGAGCAGCTTAG
Mouse Stau1 (Reverse)	CCTGCTGGATCTGTGCAAGTC
Mouse β-Actin (Forward)	GGCTGTATTCCCCTCCATCG
Mouse β-Actin (Reverse)	CCAGTTGGTAACAATGCCATGT

List of primers (continued)

Table S7. Primers used for quantitative PCR analysis (continued)

Gene	Sequence (5′ to 3′)
Human IL6 (Forward)	CAGCCACTCACCTCTTCAGAAC
Human IL6 (Reverse)	GCATCCATCTTTTTCAGCCATCTTTGG
Human TNF (Forward)	CTGCCTGCTGCACTTTGGAGTG
Human TNF (Reverse)	CATTGGCCAGGAGGGCATTGG
Human PTGS2 (Forward)	CATGTCAAAACCGAGGTGTATG
Human PTGS2 (Reverse)	GAAGTGGGTAAGTATGTAGTGCAC
Human ICOS (Forward)	CTTGGACCATTCTCATGCCAAC
Human ICOS (Reverse)	GCATCCCAAAATGCAGACTAC
Human ZC3H12A (Forward)	GAAGAGGAAAAGGAGGGCAG
Human ZC3H12A (Reverse)	CTCCAGGATGGCACAAACAC
Human Roquin (RC3H1) (Forward)	GGTTGTGGCCATACTGTCTG
Human Roquin (RC3H1) (Reverse)	GCTTTGTGTCTTCAACCCCAC
Human Roquin2 (RC3H2) (Forward)	GACCAGACTGCCATCAACAC
Human Roquin2 (RC3H2) (Reverse)	GTAGAGTGCCAAATCCTCAACG
Human NFKBIZ (IkBz) (Forward)	GAAAGGGCCCGATTCGTTGTCTG
Human NFKBIZ (IkBz) (Reverse)	GAAGCAGATCAGCACTGCTCTC
Human NFKBID (IkBNS) (Forward)	CTCCTGACTTCTACCCACCCTC
Human NFKBID (IkBNS) (Reverse)	CCAAAGCCAGCATGTGAGCTC
Human UPF1 (Forward)	GTTGAACTTCGAGGAAGATG
Human UPF1 (Reverse)	CATTTTGCCCTCACAAGGTG
Human UPF2 (Forward)	CAGAGAAACAACAGCCCTTC
Human UPF2 (Reverse)	CAGCTTCTGGTAAGACATAGC
Human UPF3x (Forward)	GAAGATAAGCAGGATCGCAAC
Human UPF3x (Reverse)	GTTGATGTATGCTCTGGCATAC
Human CXCL-1 (Forward)	GAATTCACCCCAAGAACATC
Human CXCL-1 (Reverse)	CTTCTGGTCAGTTGGATTTG
Human CXCL-2 (Forward)	GAACTGCGCTGCCAGTGCTTG
Human CXCL-2 (Reverse)	GATTTTCTTAACCATGGGCGATG
Human CXCL-3 (Forward)	GTGGTCACTGAACTGCGCTG
Human CXCL-3 (Reverse)	GATTTTCTGAACCATGGGGGATG
Human NFKBIA (IkBa) (Forward)	GAGGAGTACGAGCAGATGGTC
Human NFKBIA (IkBa) (Reverse)	CAGGTTGTTCTGGAAGTTGAG
Human GAS5 (Forward)	GTGTGGCTCTGGATAGCACC
Human GAS5 (Reverse)	GAACCATTAAGCTGGTCCAGG
Human SMG5 (Forward)	GTGCATCGACTTGACCTCATC
Human SMG5 (Reverse)	GTATACCTTTCTCCACAGCAG
Human MAFK (Forward)	CGACTAATCCCAAACCGAATAAGG
Human MAFK (Reverse)	GTTCTTGAGTGTGCGCCGAC
Human STAU1 (Forward)	CTTACTCTCGGATGCAGTCCAC
Human STAU1 (Reverse)	GATCCTCAACGCTTTGGCAG
Human β-ACTIN (Forward)	CACCATTGGCAATGAGCGGTTCC
Human β-ACTIN (Reverse)	CTTCTGCATCCTGTCGGCAATGC
Firefly Luciferase (Forward)	CTGGAAGATGGAACCGCTGGAG
Firefly Luciferase (Reverse)	CACTGCATACGACGATTCTGTG
Renilla Luciferase (Forward)	GGATGATAACTGGTCCGCAG
Renilla Luciferase (Reverse)	CACCGCGCTACTGGCTCAATATG

List of primers (continued)

Table S7. Primers used for the preparation of Northern blot probes

Gene	Sequence (5′ to 3′)
Mouse Il6 CDS (Forward)	GTTCCTCTCTGCAAGAGACTTCCATCC
Mouse Il6 CDS (Reverse)	GTATCTCTCTGAAGGACTCTGGCTTTG
Mouse β-Actin CDS (Forward)	CTATGTGGGTGACGAGGCCCAGAG
Mouse β-Actin CDS (Reverse)	GGGTACATGGTGGTACCACCAGAC
Human UPF1 CDS (Forward)	CTGTGGACGACAGTGTAGCCAAGAC
Human UPF1 CDS (Reverse)	GAGCTGTCCCAGTTGATGTCCTTGAG
Mouse β-Globin CDS (Forward)	CACCTGACTGATGCTGAGAAGGCTG
Mouse β-Globin CDS (Reverse)	CTTCTGGAAGGCAGCCTGTGCAG